Timing of deglaciation and postglacial environmental dynamics in NW Iberia: The Sanabria Lake record

Margarita Jambrina-Enríquez[1(*)], Mayte Rico[2], Ana Moreno[2], Manel Leira[3], Patricia Bernárdez[4], Ricardo Prego[5], Clemente Recio[1], Blas L. Valero-Garcés[2]

[1]Departamento de Geología, Facultad de Ciencias, Universidad de Salamanca, Plaza de los Caídos, s/n 37008 Salamanca, Spain.
margajambrina@usal.es, crecio@usal.es

[2]Instituto Pirenaico de Ecología (CSIC), Avda. Montañana 1005, 50059 Zaragoza, Spain.
mayterico@ipe.csic.es; amoreno@ipe.csic.es; blas@ipe.csic.es

[3]Centro de Geologia Universidade de Lisboa (CeGUL), Departamento de Geologia Faculdade de Ciências.Universidade de Lisboa. Bloco C6, Campo Grande, 1749-016 Lisboa, Portugal
mleira@fc.ul.pt

[4]Departamento de Geociencias Marinas y Ordenación del Territorio, Edificio de Ciencias Experimentales, Universidad de Vigo, 36310 Vigo, Spain
pbernardez@uvigo.es

[5]Instituto de Investigaciones Marinas (CSIC). Eduardo Cabello, 6. E-36208 Vigo, Spain.
prego@iim.csic.es

Key words: Lake sediments, geochemistry, XRF, diatoms, paleofloods, Late glacial, Holocene, Abrupt climate changes, Sanabria Lake, SW Europe.

* Corresponding author.
E-mail address: margajambrina@usal.es (M. Jambrina-Enríquez).

ABSTRACT

The multiproxy study (sedimentology, geochemistry and diatoms) of sediment cores from Sanabria Lake (42°07'30'' N, 06°43'00'' W, 1000 m a.s.l.) together with a robust ^{14}C chronology provides the first high-resolution and continuous sedimentary record in the region, extending back the last 26 ka. The development of a proglacial lake before 26 cal ka BP demonstrates the onset of deglaciation before the global Last Glacial Maximum, similarly to other alpine glaciers in southern European mountains. Rapid deglaciation occurred at the beginning of the Greenland Interstadial GI-1e (Bølling, 14.6 cal ka BP). Following a short-

lived episode of glacier re-advance (14.4-14.2 cal ka BP, GI-1d), a climatic improvement at 13.9 cal ka BP suggests the glaciers retreated from the lake basin during the GI-1c. Another glacier reactivation phase occurred between ca. 13.0-12.4 ka, starting earlier than the onset of GS-1 (Younger Dryas). Rapid deglaciation during the Early Holocene (11.7 to 10.1 cal ka BP) was followed by a period of higher river discharge (10.1 to 8.2 cal ka BP). After 8.2 ka, the Holocene is characterized by a general decreasing trend in humidity, punctuated by the driest phase during the Mid Holocene (ca. 6.8-4.8), a wetter interval between 4.8 and 3.3 cal ka BP, and a relatively decline of rainfall since then till present, with a minor increase in humidity during some phases (ca 1670-1760) of the Little Ice Age.

Discrete silt layers intercalated in the organic-rich Holocene deposits reflect large flooding events of the Tera River (ca 10.1, 8.4, 7.5, 6.2, 5.7-5.6, 4.6, 4.2, 3.7, 3.3, 3.1, 2.7, 2.5 and 2.0 cal ka BP). Their synchronicity with a number of cold and humid events described in the Atlantic demonstrates a strong control of NW Iberian climate by North Atlantic dynamics at centennial-millennial scale. Comparison with Western Mediterranean records points to similar regional dynamics during the Holocene, although modulated in the NW Iberian Peninsula by the stronger Atlantic influence.

1. INTRODUCTION

Climate in midlatitude regions of the western northern Atlantic seaboard and Europe is greatly influenced by high latitude (North Atlantic and Arctic oceans) dynamics (Hurrell, 1995; Cohen and Barlow, 2005) but tropical and subtropical processes have also played a significant role during the last glacial cycle (Fletcher and Sánchez-Goñi, 2008; Spöt et al., 2010). In mid latitudes, the timing and dynamics of climate changes during the Last Glacial cycle have not yet been completely resolved to evaluate the effect of low versus high latitude forcings (Menviel et al., 2014). The Iberian Peninsula (IP) has proven to be a sensitive region to short-

lived climatic shifts during the Last Glacial cycle and the Holocene, due to its location at geographic and atmospheric boundaries (Moreno et al., 2012a). Some high-resolution multiproxy analyses for the Lateglacial and Early Holocene (15.6–10.5 cal ka BP) from NW Spain (Muñoz Sobrino et al., 2013) have recently demonstrated that abrupt changes are coherent with the Greenland record and the INTIMATE stratigraphy (Lowe et al., 2008). These new records add to previous evidences of a strong control of western Iberian climate by North Atlantic dynamics during last millennia provided by marine records from the Iberian margin (e.g. de Abreu et al., 2003; Bernárdez et al., 2008; Rodrigues et al., 2010; Muñoz Sobrino et al., 2012) and continental records (mostly pollen and secondarily, diatom, biomarkers, and recently some speleothems) (see Fig. 1, with location and key references).

Available records in the western Mediterranean show a large regional variability (Carrión et al., 2010; Magny et al., 2013a, b) during deglaciation and the Holocene, likely a result of latitudinal gradients, the complex topography, and the interplay of Atlantic and Mediterranean influences. Although abrupt climate changes have been clearly identified during the Late Glacial (Fletcher and Sánchez-Goñi, 2008; Combourieu Nebout, et al., 2009) and Holocene (Mayewski et al., 2004; Wanner et al., 2008), the regional and temporal patterns and the underlying mechanisms of this variability remain unclear. New well-dated and multiproxy records from key regions located in sensitive climate transects are needed to solve the links between mid-latitude and northern climate dynamics, the peculiarities of last deglaciation and Holocene in southern latitudes, and the timing and extent of the abrupt climate changes.

Since winter atmospheric circulation variability in Western Europe is greatly associated with the North Atlantic Oscillation (NAO) (Hurrell, 1995), a NAO-like mechanism operating a centennial and even millennial scales has been proposed to explain past climate patterns, particularly during the Holocene (Nesje et al., 2001; Magny et al., 2013b; Simonneau et al.,

2013a). However, modern climate studies (Lorenzo et al., 2008; Trigo et al., 2008; González-Villanueva et al., 2013; Jerez and Trigo, 2013; Comas-Bru and McDermott, 2014) have shown that other atmospheric modes such as Scandinavian Pattern (SCA), the Eastern Atlantic (EA) and the Eastern Atlantic/Western Russia (EA/WR) and one hemispheric mode (North Hemisphere Annular Mode - NAM) explain some of the observed variability of the main synoptic weather types on Iberia and the Galicia sector (NW IP). In order to test these hypotheses, data from regions particularly sensitive to the NAO as the NW Iberian Peninsula are critical.

In spite of the relatively large number of terrestrial and marine records, our knowledge of the timing and dynamics of deglaciation in NW Iberia, the Holocene climate, and the correlation with global climate variability, is still fragmented mostly due to the scarcity of robust and highly-resolved chronologies. This paper contributes to solve the timing and dynamics of deglaciation and Holocene in NW Iberia with a new set of cores spanning the last 26 ka. Sanabria Lake (NW Spain) is a key site for developing long paleoclimate reconstructions because of its location in a transition zone between the Atlantic and Mediterranean bioclimatic regions (Luque, 2003; Rivas-Martinez et al., 2003; Muñoz Sobrino et al., 2004), the strong influence of North Atlantic dynamics in modern climate (Trigo et al., 2002; 2004), and the rapid response of some limnological properties to climate (de Hoyos 1996; de Hoyos et al., 1998; de Hoyos and Comín, 1999; Giralt et al., 2011).

Paleoecological research in the Sanabria region during the last decades has provided a number of sequences from the highlands (e.g. Laguna La Roya, Allen et al., 1996; Muñoz Sobrino et al., 2013) and the lowlands (e.g. Laguna de las Sanguijuelas, Muñoz-Sobrino et al., 2004; Lleguna, Muñoz-Sobrino et al., 2004, which corresponds to Sanabria Marsh, Allen et al., 1996) and showed millennial and centennial-scale fluctuations in continental vegetation associated to short-term climatic events since deglaciation. Previous studies on Lake Sanabria

short cores (spanning the last 6 ka) using pollen, diatom and sedimentary proxies (Luque and Juliá, 2002; Luque, 2003; Julià and Luque 2006; Julià et al., 2007), and detailed comparison of lake and watershed monitoring records with short cores for the most recent period (AD 1959-2005) (Giralt et al., 2011) have demonstrated the interplay of climatic oscillations and human impact, and revealed a geochemical response of the lacustrine system directly linked to winter precipitation and NAO dynamics. The occurrence of thin clastic silty layers intercalated with the dominant organic-rich sediments also provides an opportunity to investigate the coupled Tera River and Sanabria Lake dynamics during the Holocene.

In this paper we report the results of sedimentological, biological (diatoms) and geochemical (elemental and isotopic) analyses performed on a set of long Kullenberg cores retrieved from Sanabria Lake. They provide a continuous and complete sequence for deglaciation and Holocene dynamics focused on changes in depositional environments and the geochemical response of the lake. The reconstruction of past climate and environmental variability during the last 26,000 years is supported by a robust AMS ^{14}C chronology and provides the first high-resolution and continuous sedimentary records in the region extending back the last 26 ka, and the opportunity to investigate deglaciation and Holocene dynamics in NW Iberia, the impact of North Atlantic processes at millennial and centennial time-scales, and the potential synchronicity with Iberian and Western Mediterranean records.

2. SITE DESCRIPTION

Sanabria Lake (42º07’30’’N, 06º43’00’’W, 1000 m a.s.l.) is the largest lake of glacial origin in the Iberian Peninsula (368 ha) (Figs. 1A and B). Geomorphologic evidences and absolute dating in Sanabria region (Cowton et al., 2009; Rodríguez-Rodríguez et al., 2011, 2014; Jiménez-Sánchez et al., 2012) showed evidences of the development of an extensive ice cap in the highlands of the Trevinca Massif, that covered more than 440 km^2 during the local

Maximum Ice Extent (MIE), and developed valley glaciers reaching as low as 1000 m. The lake is located in the Parque Natural Lago de Sanabria (Zamora, NW Iberian Peninsula) in the eastern foothills of the Segundera Range (2127 m a.s.l.) (Fig. 1C and D). It is behind the main terminal moraine complex consisting of several lateral moraines more than 6 km long, nine frontal moraines, and some undifferentiated till deposits (Jiménez-Sánchez et al., 2012).

The catchment area consists of granitic rocks (Ollo de Sapo gneiss and granodiorite formations), locally covered by Quaternary glacial deposits (Rodríguez-Rodríguez et al., 2011) (Fig. 1E). Lithic Leptosols and thin umbric Leptosols dominate in the catchment area while umbric Gleysols predominate in the highlands; soils around the Lake are humid Cambisols and eutric Fluvisols (Atlas Agroclimático de Castilla y León, 2013) (Fig. 1F). The watershed vegetation shows a clear altitudinal distribution: shrubs and pastures in highplains, a *Quercus pyrenaica* woodland with patches of *Pinus sylvestris* - which at present are repopulations - *Juniperus oxycedrus, Taxus baccata,* and *Ilex aquifolium* between 1500 and 1700 m a.s.l., and a *Quercus ilex* forest below 1500 m a.s.l. (Julià et al., 2007). The open landscapes in the western (Tera River inlet) and northern shorelines (S. Martin de Castañeda) are associated with managed pastures (Luque, 2003, Julià et al., 2007) (Figs. 1G and H). Vegetation around the lake consists of *Populus nigra, Alnus glutinosa, Fraxinus angustifolia* and *Salix* spp. (Vega et al., 1992, Luque, 2003, Julià et al., 2007). The littoral zone is colonized by a well-developed aquatic plant community (mostly limnophytes, helophytes and amphyphytes) (Julià et al., 2007).

Sanabria Lake is a hydrologically open lake situated in the Tera River exoreic drainage basin (127.3 km^2). The Tera River is the principal inflow and the only natural outflow. It runs southward from Peña Trevinca peak (2127 m a.s.l, northern end of the Segundera Range) through the highland plateau (slope of 3%) and the Tera Canyon (11-20% slope) to the

Ribadelago village (1000 m a.s.l.), where receives the Cardena and Segundera tributaries and turns east into the Sanabria Lake (Figs. 1C and D). Although, the Tera River is regulated since 1950s by six reservoirs upstream the lake, river flow, water and sediment delivery into the lake are strongly linked to precipitation (de Hoyos, 1996; Giralt et al., 2011).

The Sanabria region has a continental climate with Atlantic influence and two main bioclimate variant controlled by altitude and geographic location (Rivas-Martínez et al., 2003). The highlands with Oromediterranean climate are characterized by higher annual precipitations (1568 mm), colder mean annual temperature (6ºC) and significant snowfall in winter above 1500 m a.s.l. The lowlands are Supramediterranean with relatively lower annual precipitation (1465 mm) and warmer mean annual temperature (10ºC) (36 year meteorological series, Presa Cardena - 1600 m a.s.l. - and Ribadelago - 1000 m a.s.l. - weather stations; data supplied by J.C. Vega, from the *Laboratorio Limnológico Lago de Sanabria, JCyL*). Most of the precipitation is related to Atlantic fronts during the winter months (with a relatively high interannual variability), strongly controlled by the NAO (Trigo et al., 2002, 2004) with positive averages of the standardized precipitation index (SPI) associated with negative NAO mode (Vicente-Serrano and López-Moreno, 2008). Other patterns such as EA, EA/WR and SCA explain some of the climate variabiity in Galicia (NW Iberia) during other seasons (Lorenzo et al., 2008).

Sanabria Lake has a maximum length of 3.16 km W to E, along the pre-glacial fluvial valley, a maximum width of 1.53 km, and a volume of 96 Hm^3; the lake bathymetry shows two over excavated sub-basins (of 51 –eastern- and 45 m –western- maximum depth) separated by a ridge 20 m below the water surface (Vega et al., 2005). The lake is warm (4.5-24.8ºC water temperature), oligotrophic and monomictic, thermally stratified from March to November (de Hoyos, 1996). Its water is slightly acidic (annual average pH=6.2), with low alkalinity

(average 0.045 meq·L^{-1}) and low ion content (annual average conductivity is 14.9 µS·cm^{-1}) (de Hoyos and Comín, 1999). Water residence time is about 5-9 months, and the whole column is oxygenated through the year (de Hoyos, 1996; de Hoyos and Comín, 1999). The phytoplankton community is composed of Cryptophyta, Chlorophyta, Cyanobacteria; diatoms (main species *Aulacoseira distans, Cyclotella glomerata and Cyclotella stelligera*) are less abundant (around 1% of total algae, Aldasoro et al., 1991, de Hoyos and Comín, 1999; Negro et al., 2000). Lake productivity and phytoplankton are highly sensitive to the seasonal nutrient input influenced by rainfall regimes and consequently by the NAO variability (de Hoyos, 1996; Luque and Julià, 2002; Giralt et al., 2011).

3. METHODS

Five sediment cores were retrieved in 2004 using a Kullenberg piston coring equipment and platform from the Limnological Research Center (LRC), University of Minnesota (USA): two from the eastern sub-basin (2A, 7.7 m-long and 3A, 8.9 m-long) and three from the western sub-basin (1A, 5.9 m-long; 1B, 7.4 m-long and 4A, 5.8 m-long) (Figs. 2 and 3). Two additional Uwitec® short-cores (1M, 39 cm-long and 2M, 64 cm-long) from the eastern sub-basin were obtained in 2007 to reconstruct the uppermost part of the sequence (Figs. 2 and 3). Magnetic susceptibility (MS) was measured every 1 cm for all the cores, using a Geotek Multi Sensor Core Logger (MSCL) at the Limnological Research Center (LRC), University of Minnesota (USA). The cores were split into two halves and imaged with a DMT Core Scanner to obtain high-resolution photographs and digital color parameters as Lightness (L*) following LRC procedures. Sedimentary facies were identified by visual observations including color, lithology and sedimentary structures (Schnurrenberger et al., 2003).

The longest core (3A, 8.9 m-long) and the short core 2M (64 cm-long), both retrieved in the deepest eastern sub-basin (Zmax=51 m deep; Fig. 2), were selected for detailed studies. The

cores were sub-sampled for Total Organic Carbon (TOC), Total Nitrogen (TN), $\delta^{13}C_{org}$ and for biogenic silica (BioSi) analysis every 5 cm (core 3A) or every 1 cm (core 2M). TOC was analyzed with a LECO SC 144DR furnace, and TN was measured using a VARIO MAX CN elemental analyzer, both at the Instituto Pirenaico de Ecología (IPE-CSIC), Spain. Inorganic carbon in these sediments is below detection limit, so Total Carbon measurements actually represent the Total Organic Carbon. C/N is expressed as atomic ratio. Samples for BioSi were prepared using approximately 50 mg of dried sediment, which was treated with 5 mL of 1N HCl and 5 mL of 10 vol H_2O_2 to remove carbonates and organic matter. BioSi was extracted into a 2M Na_2CO_3 solution at 85°C for 5 h. Silica was measured photometrically according to the method of Hansen and Grasshoff (1983) using a continuous flow analyzer AutoAnalyser Technicon II analyzer at the Instituto de Investigaciones Marinas (IIM-CSIC), Spain. Precision of the biogenic silica measurement is evaluated from replicate analyses of surface samples giving a coefficient of variability (e.g. standard deviation) of ±0.2 (Bernárdez et al., 2005). Samples for grain size were taken every 1 cm from short core 2M and treated with hydrogen peroxide to eliminate organic matter and a dispersant agent prior to measurement with a LS-13-320 Beckman Coulter Counter at the Departamento de Estratigrafía, Paleontología y Geociencias Marinas, Universidad de Barcelona, Spain.

The $^{13}C/^{12}C$ ratios of organic matter were measured at the Laboratorio de Isótopos Estables, Universidad de Salamanca, Spain, on CO_2 obtained by combustion on a EuroVector EA3000 elemental analyser coupled on-line to an Isoprime continuous flow mass spectrometer. Samples of 1-3 g of wet sediment were treated with excess 1N HCl to remove carbonate, washed with distilled water and dried at 40ºC following Sofer's (1980) method. Samples were crushed in an agate mortar to reduce the grain size and homogenize and then weighted and encapsulated in triplicate in tin capsules. All isotopic analyses were done in triplicate. Results

are expressed as δ *per mil* values relative to PDB (Pee Dee Belemnite) standard (Craig, 1957). The analytical precision is always better than ±0.1‰.

X-Ray Fleuorescence data (XRF) (core 3A, 5 mm resolution) were obtained with an ITRAX core scanner (Croudace et al., 2006) from the Large Lake Observatory (University of Minnesota, USA). The XRF settings were 45 kV, 30 mA and 30 s exposure time using Mo and Cr tubes to obtain statistically significant values for K, Ti, Fe, Sr, Si, As, Ca and Mn. The results are expressed as peak areas. Two intervals of the sediment sequence (63-23 and 220-160 depth cm) could not be analyzed due to bad preservation of core sediment surface.

Taxonomic identification and quantification of diatoms was carried out in 28 samples in core 3A (every 30 cm approximately between 874 and 59 cm depth) and 18 samples in core 2M (every 10 cm between 61and 22 cm depth, every 2 cm between 22 and 9 cm depth, and every 1 cm until top of the core). Diatom slides were prepared following standard procedures (Battarbee et al., 2001). Specimens were mounted in Naphrax and whenever possible at least 300-500 valves were counted in each sample. Valve concentrations per unit weight of sediment were calculated using DVB (divinylbenzene) microspheres (Battarbee, 1986) and transformed to diatom fluxes (valves cm^{-1} yr^{-1}). When diatom content was lower than 300, counting continued until reaching at least 1000 microspheres or until the frequency of the taxa in the sample count stabilizes in relation to the overall size of the sample count (Battarbee et al., 2001). Taxonomic identifications were made using specialized literature (Lange-Bertalot, 2000-2011; Houk, 2003; Houk et al., 2010).

The chronology for core 2M has been constrained using ^{210}Pb techniques for the upper 30.5 cm depth at the St. Croix Watershed Reseach Station, Science Museum of Minnesota (USA) and one ^{14}C AMS date at 36.5 cm depth obtained at the Poznan Radiocarbon Laboratory, Poland and calibrated using the IntCal13 curve (Table 1). The ^{210}Pb chronology for the core

was determined by the c.r.s. (constant rate of supply) model, which assumes constant input of excess ^{210}Pb to the core site, but allows sediment flux to vary. Dating uncertainty increases substantially in the lowermost intervals, largely because of the high and somewhat variable values for supported ^{210}Pb, and exceeds ± 20 years for dates older than ca 1900. The age-depth model for the short core was established using CLAM software and a smooth cubic spline (type 4) with a smoothing value of 0.3 and 10000 iterations (Blaauw, 2010). The model also includes as a key horizon the sand-silt layer at 12-20 cm depth deposited during the flash flood after the Vega de Tera Dam-failure in 1959 AD (Julià et al. 2007; Giralt et al., 2011).

Chronology for the long core 3A is constrained by 13 ^{14}C AMS dates on terrestrial macro remains and bulk organic matter (Table 1), analyzed in the Poznan Radiocarbon Laboratory, Poland. The dates were calibrated using CALIB program (Stuiver et al., 2005), with the IntCal13 calibration curve at two sigma probability (Reimer et al., 2013) and the depth-age model was constructed using a generalized mixed-effect regression function (Heegaard et al., 2005). Only one date was rejected because it was too old for its stratigraphic location, likely as a result of reworking of older sediment (Table 1).

4. RESULTS

4.1. Chronology

According to the age model, core 3A spans from 25.6 cal ka BP to 810 cal yr BP (Fig. 4). Lake sedimentation rate (L.S.R.) is the lowest (L.S.R.=0.14 mm yr^{-1}) at the base of the sequence (ca 26–14 cal ka BP) and increases (L.S.R.=0.21 mm yr^{-1}) with the onset of more organic deposition at 14 ka. The Holocene L.S.R during the Early and Mid-Holocene is 0.47 mm yr^{-1} on average, and increases to 1.20 mm yr^{-1} during the last 3.3 ka (Fig. 4A).

The chronology of the upper 36.5 cm of the short core 2M is better constrained and spans between AD 2005 and 1770. The chronology of the lower half (36.5-63.5 cm) has a larger uncertainty and assuming the same sedimentation rate (1.08 mm yr^{-1}) obtained for top subunit 1A in core 3A (AD 1140-686) the base of core 2M has an AD ca 1520 age (Fig. 4B). Sediment accumulation rates are relatively uniform (between 0.3 and 0.5 g cm^{-2} yr^{-1}) excluding the section corresponding to the 1959 dam failure when they spike by two orders of magnitude. The calculated flux of excess ^{210}Pb to the core site (0.78 pCi cm^{-2} yr^{-1}) exceeds expected atmospheric deposition rates for ^{210}Pb in this region by approximately a factor of two, indicating significant focusing of sediments to the deepest eastern sub-basin (Zmax=51 m deep) where the core was collected (Fig. 4C).

4.2. Sedimentary facies

Eight sedimentary facies have been defined using sedimentological properties (grain size and sedimentary structures), lithology, color and lightness, sediment composition (TOC, TN, BioSi), geochemical composition (XRF data), smear slide observations and magnetic susceptibility (Table 2 and Figs. 5 and 6). They group in three associations (i) clastic, (ii) clastic-organic and (iii) organic facies.

Recent sedimentation in Lake Sanabria is controlled by two main factors: i) the sediment input from the Tera River and ii) the organic productivity in the littoral (mostly macrophytes) and distal (algal) areas (de Hoyos et al.,1998; Giralt et al., 2011). Statistical approaches such as factor analysis and principal component analysis (PCA) in short cores (Luque, 2003; Juliá and Luque, 2006; Giralt et al., 2011) revealed that increased terrigenous input to the lake characterized by higher silicate content and higher values of K, Ti, Si, Fe and Sr occurred during periods of higher Tera River flow and rainfall. Lacustrine sediments with lower fluvial influence are more organic–rich and with higher S, P and Mn values (Giralt et al., 2011).

Sediment composition (mineralogy and organic matter content), physical properties (MS and L*) and chemical composition characterize the clastic input to the lake (Fig. 6). Higher L* values coincide with intervals of coarser-grained layers (sandy silts) and facies H, characterized by higher MS and lower TOC whereas lower L* correspond with organic-rich facies F. Low MS values occur throughout most of the sequence dominated by organic matter-rich silts (facies F). Basal coarse facies A and B, fine sand facies E, and intercalated thin clastic facies Ha show moderate to high MS values. Higher XRF values (Si, K, Fe, Ti) and elemental ratios (Mn/Fe, Si/Ti, Sr/Ti, Ca/Ti) identify clastic facies. The Mn/Fe ratio is proxy for syn- and post-depositional redox conditions in the bottom waters and sediment in lacustrine systems (e.g., Naeher et al., 2013). The Si/Ti ratio reflects the biogenic (diatom productivity) versus clastic input. In absence of a carbonate catchment area, normalization of Ca and Sr with Ti informs about silicate weathering and sediment input to the lake (Cohen, 2003).

The three facies associations in core 3A and 2M represent sedimentation in the distal area of the Lake (eastern sub-basin). The clastic facies (facies A and B, Table 2) are made of sandy and silty sediments, composed by quartz, micas, feldespars and clay minerals. MS, L*, and detrital-related elements (K, Ti, see below) show the highest values of the sequence in these facies. TOC and BioSi contents are the lowest. These facies are similar to proglacial sediments in lakes from recently deglaciated areas (Nesje et al., 2001; Chapron et al., 2007) and basal sediment in most Iberian glacial lakes (e.g., small lakes in Sanabria region, Muñoz-Sobrino et al., 2004, 2005, 2007, 2013; Portalet, González-Sampériz et al., 2006; Villaseca, Jalut et al., 2010; Enol, Moreno et al., 2011).

The clastic-organic facies (facies C, D and E, Table 2) include (i) laminated organic silts (facies C and D) with lower MS and L*, higher organic and BioSi content, and moderate

content in detrital-related elements (K, Ti); and (ii) fine sand and silt layers (facies E) with major amounts of quartz, feldspars and mica, higher MS, L*, K and Ti values and lower organic and BioSi content. These sediments are interpreted as deposited in a glaciolacustrine environment with periods of higher clastic delivery (facies E) associated to higher Tera glacier meltwater input.

The organic-rich facies (facies F, G and H) occur as (i) massive fine organic-rich silts and oozes (facies F) characterized by higher TOC and BioSi values, and lower MS (average 6 SI) L*, K, Ti, and finer grain size, (ii) laminated to banded silts layers (facies G) with variable TOC and BioSi content, and higher MS, L* and K, Ti values, (iii) coarser sandy layer (facies H) characterized by higher MS, L*, K, Ti and grain size values, and lower TOC and BioSi content. The intercalated facies Ha are singled out by their relatively higher values in Si, K, Fe and Ti. Facies F represents deposition in the distal, deep areas of lake Sanabria, dominated by organic processes. Facies G represent periods with higher fluvial influence, although still dominated by organic deposition. Facies H are interpreted as fine silts deposited in the distal areas of the lake during flood events of the Tera River. Facies G and Ha are similar to inorganic-rich sandy layers (Munsell color: 7.5YR, mean grain size=30μm, higher Sr, Ti, K, Al and lower Loss on Ignition-LOI, TOC, TN, P, S and Mn) described by Luque (2003) and Julià and Luque (2006) in Sanabria cores. The AD 1959 event layer has been identified in all short cores as a coarsening upward sequence (facies Hb) (Luque and Julià, 2002; Luque, 2003; Juliá and Luque 2006; Giralt et al., 2011). Its geochemical composition with higher content of Ca, Na and Ni than previous Ha facies has been related to the presence of dam material (concrete) (Luque and Julià, 2002; Luque, 2003; Juliá and Luque 2006).

4.3. The Sedimentary sequence

The Sanabria sequence has been divided into three sedimentary units according to sedimentary facies, magnetic susceptibility, lightness and geochemical composition (XRF) (Figs 5, 6 and 7). The cores from the two sub-basins have been correlated using sedimentary facies, the occurrence of key distinctive layers and magnetic susceptibility profiles (Fig. 3):

Unit 3 (890-729 cm depth, 25.5-13.9 cal ka BP) is made of light grey sand and silt layers (facies A and B) with the highest MS (15-28x10^{-5} SI), K (from 8300 to 16300 peak area), Ti (from 4144 to 7070 peak area) and L* (51-87) and the lowest TOC (<0.3%), TN (<0.06%) and BioSi (<0.9%) contents of the whole sequence. This unit shows a wide range of $\delta^{13}C_{org}$ values (-22.4 to -14.7‰).

Unit 2 (729-670 cm depth, 13.9-11.2 cal ka BP) is composed of the organic–clastic facies association (facies C, D and E):

Subunit 2C (729-713 cm depth, 13.9-13.0 cal ka BP) is made up of organic dark gray silts (facies C), and is characterized by a small increase in organic content (TOC=2.4%; TN=0.6%, C/N=9.8, $\delta^{13}C_{org}$=-26.0‰, BioSi=2.5%) and low MS (8.1-12.0x10^{-5} SI) and L* (22.0-41.7). K and Ti values are relatively high (K=4551-5759 peak area; Ti=3187-4551 peak area) and decrease upwards.

Subunit 2B (713-701 cm depth, 13.0–12.4 cal ka BP) is a fining upward sequence of gray sand and sandy silt (facies E) with higher MS (8.8-12.3x10^{-5} SI) and L* (11.7-60.1). The onset is marked by peaks of K (9709 peak area) and Ti (4989 peak area) at 713 cm (13.0 cal ka BP), associated to clastic facies E. The organic content is variable, with lower values in the sand facies (TOC=3.0%; TN=0.3%; BioSi=1.7%) and higher in the fine silts layers (TOC=7.3%; TN=0.6%; BioSi=3.5%). $\delta^{13}C_{org}$ and C/N values vary in a narrow range from -26.5 to -26.1‰ and from 13.0 to 13.9 respectively.

Subunit 2A (701-670 cm depth, 12.4-11.2 cal ka BP) is composed by organic-rich silts (facies D). Lower organic matter content (TOC=4.0, TN=0.5, C/N=8.3; $\delta^{13}C_{org}$=-27.1‰) and higher BioSi values (9.8%) occurred at the onset of the subunit (701-688 cm; 12.4-11.8 cal ka BP). Organic-related parameters increased towards the top (TOC=5.3, TN=0.6, C/N=10.4; $\delta^{13}C_{org}$=-26.8‰). Subunit 2A has a distinctive geochemical signature with the lowest K (from 1500 to 2000 peak area) and Ti (from 900 to 1200 peak area) values and the highest As (from 3400 to 8000 peak area). The Si/Ti and Ca/Ti ratios are higher and the Sr/Ti lower than in other units.

Unit 1 (670–0 cm, 11.2-0.81 cal ka BP) is made of organic facies (facies F) with intercalated clastic layers (facies G and Ha). Subunit 1E and 1C are dominated by deposition of facies G and show higher frequency of facies Ha. Subunits 1D and 1B are composed of organic-rich facies F with some clastic facies Ha. Finally, subunit 1A is also composed of facies F but with higher MS values. The geochemistry of the Holocene sediments (unit 1) is controlled by the characteristics of dominant organic–rich facies F. The intercalated facies Ha are singled out by their relatively higher values in Si, K, Fe and Ti.

Subunit 1E (670-511 cm, 11.2–6.8 cal ka BP) starts with several sandy silt layers at the base (facies Ha and G) (670-573 cm; 11.1-8.2 cal ka BP) grading to more organic–rich fine silts (facies G) towards the top with some intercalated clastic layers (facies Ha) at 643 cm (10.1 cal ka BP) and at 543 cm (7.5 cal ka BP). The subunit has high K (1700-9100 peak area), As (1200-5300 peak area) and Sr/Ti ratio and lower Mn/Fe. The organic content shows an increasing trend (TOC between 2.6 and 11.6%, TN between 0.3-0.9%; C/N between 11.7 and14.9). $\delta^{13}C_{org}$ varies between -26.2 and -27.1‰. BioSi is higher at the base (670-643 cm, 11.1-10.1 cal ka BP) and declines upward (8.3-3.8%).

Subunit 1D (511-417 cm, 6.8–4.8 cal ka BP) is dominated by the sedimentation of organic-rich silts (facies F) with low MS (4.1-5.5x10^{-5} SI) and L* (1.6-7.1) values, with fewer coarser clastics (facies Ha), higher Si/Ti ratio but lower Sr/Ti. Organic content shows an increasing trend (TOC=8.9-12.8, TN=0.8-1.0%). C/N and $\delta^{13}C_{org}$ remain stable (C/N=14.1-14.5; $\delta^{13}C_{org=}$ -26.8‰).

Subunit 1C (417-309 cm, 4.8–3.3 cal ka BP) is composed of laminated to banded silts (facies G) and a basal sandy layer (facies Ha). It is characterized by higher MS (average 5.1x10^{-5} SI), L* (average value 4.5), K (1500-4500 peak area), Ti (1136-4190 peak area) and Sr/Ti ratios and lower As (517-1500 peak area).

Subunit 1B (309-50 cm, 3.3–1.26 cal ka BP) is dominated by organic-rich facies F (TOC=5.0-11.7%; TN=0.4-0.9%, C/N=17.1-13.4, $\delta^{13}C_{org}$=-27.8 to -26.4‰) and coarser clastic facies Ha, and characterized by an upward increasing trend of MS (5.1-10.4x10^{-5} SI) and L* (4.2-19.2), higher Mn/Fe and lower Sr/Ti and Si/Ti ratios.

Finally, subunit 1A (50-0 cm depth, 1259-817 cal yr BP in core 3A and 63.5 to 0 cm depth, AD 1522-2007 in core 2A) is mostly composed of facies F, with few G and H levels. The subunit has generally higher organic content (TOC=9.2-12.5%; TN=0.7-1%; C/N=13.8-15.3; $\delta^{13}C_{org}$=-27.9 to -26.2‰), higher MS values (7.0-13.2x10^{-5} SI) and relatively higher K (1060-2700 peak area) and Ti (1400-2600 peak area) (Figs. 6 and 7). The AD 1959 event layer, identified in all short cores, corresponds to a coarsening upward sequence (Facies Hb) with the lowest organic content (TOC=5.3%; TN=0.4%; C/N=15.1). After AD 1959 the sedimentation comprises organic-rich silts and silty layers (facies F and G) with higher organic content (TOC=7.4%; TN=0.7%; C/N=14.4; BioSi=1.9%; $\delta^{13}C_{org}$= -27.2‰), lower mean grain size (mean value is 28.1 μm), a decrease in lithogenic elements (K, Si, Ti, Sr, Ca,) (Fig. 7), and an increase in S, Mn and P (Giralt et al., 2011).

4.4. Diatoms

Diatom concentration varies from $1.5x10^6$ to $57.7x10^6$ "valves.gr^{-1}" in long core 3A and between $0.1x10^6$ and $4.2x10^6$ "valves.gr^{-1}" in short core 2M (Fig. 8). The most abundant species are *Aulacoseira subborealis* and *Tabellaria flocculosa* var. *linearis* for core 3A, and *A. subborealis* and *Cyclotella stelligera* for core 2M. Diatom concentration and BioSi content show parallel trends in both the long (Fig. 8) and short (Fig. 7) cores.

In long core 3A, diatoms are absent in Unit 3 and scarce in subunits 2B and 2C, dominated by *Aulacoseira valida* (40%) (Fig.8). Diatom preservation was also relatively poor, and many specimens were affected by fragmentation and/or dissolution. Nevertheless, the most representative taxa could be identified reliably while for most of the other taxa, easily identifiable areas remained relatively well preserved, and hence preservation did not interfere with counting accuracy. The largest increase in diatom concentration occurred during subunit 2A associated to high biogenic silica content and dominance of planktonic *A. subborealis* (85%). Subunits 1E and 1D show a general decreasing trend of *A. subborealis* (from 85 to 10%) at the time that tychoplanktonic (*T. flocculosa* var. *linearis*) and benthic *Surirella angusta* varieties become more frequent. At the top of subunit 1D *A. subborealis* proportions increase again up to 60 %. Subunit 1C is characterized by an increase in *T. flocculosa* var. *linearis* (up to 60%) and the lowest values of *A. subborealis* (ca. 2%). After the onset of subunit 1B *A. subborealis* increases again and dominates till the top of the core, punctuated by two short periods with higher percentages of benthic *Fragilaria arcus*.

The diatom assemblage in core 2M is dominated by *A. subborealis* (60%), *Achnanthidium minutissimum* (10%) and *F. arcus* (10%) during the period AD 1520-1959. The AD 1959 event shows a unique signature: a decrease in the percentage of *A. subborealis* (20%), the first occurrence of *Cyclotella meneghiniana* (10%) and *C. stelligera* (20%), and maximum values

of benthic *F. arcus* (30%). Diatom concentration decreased after the 1959 event and the assemblages have since been dominated by fluctuations between *A. subborealis* and *C. stelligera*. Benthic diatoms such as *F. arcus* decreased ca. 5%, while *Fragilaria capucina*, *Pinnularia subcapitata* and *Staurosira construens* increased (Fig. 7).

5. Discussion

The sedimentological, geochemical and biological Sanabria dataset constrained by the robust ^{14}C age model provides the first multiproxy-based reconstruction of the timing and dynamics of the last deglaciation and the Holocene climate variability in the NW Iberian Peninsula. To describe this evolution and to evaluate the correlation with other local, regional and global records we have divided the Sanabria record in several stages.

5.1. An early onset of deglaciation: a proglacial stage (25.6-14.6 cal ka BP)

Sanabria Lake (1000 m a.s.l) formed in the inner side of the Sanabria moraine complex (at the end of the Tera Valley) occupying a 3.5 km^2 basin deepened by the glaciers. Sedimentological features of basal sediment (unit 3) point to a proglacial depositional setting. Deposition of massive silts with sand pockets (facies A and B, Table 2) would suggest that at least the eastern Sanabria Lake sub-basin was already free of glacial ice before 26 cal ka BP, although the lake dynamics were still controlled by melting glaciers in the watershed (Figs. 5 and 6). The possibility of a subglacier lake underneath the Tera glacier in the eastern sub-basin seems unlikely considering the relatively small depth of the sub-basin, and the presence of oxidized layers and pockets in the sediments pointing to well oxygenated waters. The basal age of ca. 26 cal ka BP indicates that the maximum extension of the Tera valley glacier occurred well before the global Last Glacial Maximum (LGM), centered at 21 ka cal BP (Ehlers and Gibbard, 2007). This chronology is in agreement with ages for the regional Maximum Ice Extent (MIE) in the Trevinca Massif and the Cantabrian Range (Jiménez-Sánchez and Farias,

2002; Moreno et al., 2010a; Jalut et al., 2010; Jiménez-Sánchez et al., 2012; Rodríguez-Rodríguez et al., 2011, 2014), the Gredos Range in the Central Range (Domínguez-Villar et al., 2013) and the Pyrenees (García-Ruiz et al., 2013), and support a MIE in Iberian Mountains earlier than the global LGM. Based on geomorphological evidence, during the two local MIE (> 33 ka and during the LGM of MIS 2) the Tera glacier front descended to 940 m, reaching 6.8 km in length and 2.9 km in width; and progressively was reduced, receding about 2.8 km in length and almost 2 km in width, covering only the western sub-basin around 25.6 ka BP (Rodríguez-Rodríguez et al., 2011). Ten episodes of glacier front retreat and stabilization took place after the local Maximum Ice Extent (Rodríguez-Rodríguez et al., 2011) and had been recently dated between 19.2 and 15.4 ^{10}Be ka (Rodríguez-Rodríguez et al., 2014). A nearby core (SAN08-SM1) retrieved from an ice-dammed deposit formed behind the MIE lateral moraine at San Martin de Castañeda (1250 m a.s.l.) (Fig. 1C) encountered laminated to banded fine sands and silts with some intercalated gravel layers, also interpreted as glaciolacustrine sediments, between ca 21.8 and 10.5 cal ka BP (Rodríguez-Rodríguez et al., 2011). Although this core did not reach the bottom of the San Martin de Castañeda marginal deposit, the AMS ^{14}C basal date (21,833±358 cal yr BP) demonstrates that the Tera glacier's lateral moraine had effectively blocked the creek at least by 22 ka BP (Jiménez-Sánchez et al., 2012). The Lleguna site, a small lake in the Sanabria lowlands (1050 m a.s.l, Fig. 1C), also contains a basal section of laminated clastic sediments (zonation LLE-1, from 19.1 to 18.4 cal ka BP), likely generated by melting ice (Muñoz-Sobrino et al., 2004, 2007). No laminated sediments have been identified in the sequence of Laguna de las Sanguijuelas, a small lake situated in a morainal depression northwest of Sanabria Lake (1080 m a.s.l.) (Fig. 1C), with a basal age of ca 18.6 cal ka BP (Muñoz Sobrino et al., 2004, 2007).

Compositional parameters from facies A (Table 2) are indicative of a proglacial lake with low productivity, and with no significant organic input from a glaciated watershed (Fig. 5). The

low C/N (C/N<11) ratio suggests that the scarce organic matter in the sediment derives from phytoplankton (C/N<10). However, the low organic matter content could cause artifacts in the C/N ratio (Meyers, 2003). Similar characteristics (low TOC, TN and C/N, and higher $\delta^{13}C_{org}$ and MS) were recorded at the LGM in the central Sierra Nevada (USA) and interpreted as high detrital input from alpine glaciers in the drainage, due to sparse watershed vegetation, and high meltwater runoff (Street et al., 2012). The decreasing upward trend in Si, Fe, Ti and K and also MS values (Fig. 6) and the increasing upward trend in C/N ratio and TOC at the end of the unit are coherent with diminishing detrital input by the Tera glacier, due to its progressive retreat and could reflect a more vegetated watershed as deglaciation progresses.

Pollen and chironomid data from nearby sites are also indicative of colder climates and sparsely vegetated watershed. Pollen records from Lleguna and Laguna de las Sanguijuelas (Muñoz Sobrino et al., 2004, 2007) indicate cold temperatures and/or drier conditions during the global LGM, with a steppe vegetation dominated by *Gramineae*, *Artemisia* and *Chenopodiaceae*, and increased presence of trees and shrubs (*Pinus*, *Betula*, *Juniperus*, *Cistaceae* and *Leguminosae*) during deglaciation, with the onset of regional tree succession around 16.3-15.1 cal ka BP (Muñoz Sobrino et al., 2004). Higher altitude areas of Sierra Segundera (>2100 m) could have acted as refuges offering the minimum precipitation requirements to support pine woods at mid-slope positions during the dry phases of the Lateglacial (Muñoz Sobrino et al., 2013). In the highlands (Laguna de la Roya, 1608 m a.s.l., Fig. 1C) chironomid-inferred summer temperatures were cooler and below 10ºC between 15.5 and 14.7 cal ka BP, and the pollen data indicate a catchment covered by heliophilous herbs and sparse juniper scrub from 15.5 to 14.5 cal ka BP, and the regional presence of pine woodlands between 15.2 and 14.5 cal ka BP (Muñoz Sobrino et al., 2013).

Three conspicuous episodes are well marked by sedimentological, organic and inorganic geochemical proxies. Abrupt $\delta^{13}C_{org}$ positive excursions from background -24‰ to -14.7‰ at

844 cm, -14.8‰ at 804 cm and -15.7‰ at 765 cm depth correspond with facies B (Table 2) (Figs. 5 and 6). The $\delta^{13}C_{org}$ values in lacustrine systems respond to the balance between the terrestrial (allochtonous) and lacustrine (autochthonous) organic matter, the effects of reduced availability of dissolved CO_2atm and changes in organic productivity (Hollander and MacKenzie, 1991; Meyers, 2003). However, the close correspondence with clastic events and lower BioSi content (<1%) favors the interpretation of higher $\delta^{13}C_{org}$ values in proglacial Sanabria Lake as associated to an increase in the supply of allochtonous organic matter and reduced lake productivity, likely reflecting input from a sparsely-vegetated post-glacial watershed and cold temperatures. Although age uncertainty is large in Unit 3, according to the age model, these three distinctive episodes of increased sediment delivery to the lake occurred at 21.8, 18.7 and 16.0 (Heinrich event 1, HE1) cal ka BP. Local pollen records show some rapid changes in vegetation during the Lateglacial. For example, variations in *Gramineae* percentages in the Sanabria's lowlands show peaks at ca 19.1 and 18.1 cal ka BP (with *Artemisia* <30% and <20%) and ca 16.6 cal ka BP (Lleguna) and ca 16.0 cal ka BP (Laguna de las Sanguijuelas) (Muñoz Sobrino et al., 2004, 2007).

At a regional scale, several Iberian records show abrupt changes prior to the LGM. In the north- (de Abreu et al., 2003; Naughton et al., 2007) and south- (Rodrigues et al., 2010) western Iberian Margin (Fig. 1A), oceanic deep cores recorded colder and more arid climate conditions between 31 and 23 cal ka BP, particularly during Heinrich events (HE), than during the LGM. Similarly, paleoclimatic reconstruction from northern Iberia speleothems (Fig. 1B) (Pindal cave, Moreno et al., 2010b; Eagle cave; Domínguez-Villar et al., 2013) and northern lacustrine sequences (Estanya Lake, Morellón, et al., 2009; Ayoó mire, Morales-Molino and García-Antón, 2013) show drier and colder conditions associated to some HEs. At Enol Lake (Northern IP), abrupt changes were documented in the sediment cores during the last

glaciation but age uncertainties precluded the unambiguous adscription to HE (Moreno et al., 2010a).

In any case, the clear correspondence between $\delta^{13}C_{org}$, C/N, clastic-related elements and MS during the excursions in proglacial Sanabria Lake, supports their interpretation as periods of higher input of coarser material and allochtonous organic matter into the lake, supplied by the melting waters of Tera glacier. Increased sediment input to the Sanabria proglacial Lake could reflect higher meltwater discharge from the Tera glacier (increasing melting, receding glacier) but the occurrence of coarse facies favor closer proximity of the glacier front to the coring site (glacier advance). Therefore, and in spite of the dating uncertainties, the Sanabria record demonstrates the occurrence of rapid changes during deglaciation characterized by increased sediment delivery to the lake associated to glacier dynamics.

5.2. The GI- 1 interstadial (Bølling – Allerød): a glacio-lacustrine stage (14.6-13.0 cal ka BP).

At the beginning of the Greenland Interstadial 1 (14.6 cal ka BP, onset of the Bølling period) (Lowe et al., 2008), the glacial influence in Sanabria Lake was still very strong as reflected by the deposition of siliciclastic silts with low organic content and low BioSi concentrations (facies A) during GI-1e (Figs. 5 and 6). Deposition of a coarser clastic layer (facies B) at ca 14.4-14.2 cal ka BP is interpreted as glacier reactivation in the watershed with glacier front advance in the Sanabria basin. This change in glacier dynamics may correlate with the GI-1d event in the Greenland stratigraphy (Lowe et al., 2008). Severe drought affected the Sanabria's lowlands during this period as indicated by higher values of *Artemisia* (Laguna de la Sanguijuelas, ca 15.6-14.0 cal ka BP); although, in contrast, *Pinus* peaks to >85% in Lleguna due to topographic variability (Muñoz Sobrino et al., 2004, 2007). A short cooling stage was identified by the decline of the tree pollen percentages recorded at Laguna de la

Roya (Muñoz Sobrino et al., 2013) during the GI-1d event. Speleothems from the Cantabrian Mountains (Pindal cave, Moreno et al. 2010a) also identified GI-1d event as a cold and dry period.

A short climatic improvement occurred during the Allerød (13.9-13.1 cal yr BP, ca GI-1c) and in Sanabria it was marked by a distinctive limnological change with the onset of subunit 2C and deposition of more organic, dark gray silt (facies C, Table 2), indicative of an increase in lake bioproductivity (Figs. 5, 6 and 9). The diatom communities were dominated by the planktonic centric diatom *A. valida*, more common in low temperature environments (Denys, 1991-1992) (Fig. 8). According to Houk (2003), *A. valida* is a Nordic-alpine cosmopolitan species, relatively infrequent, occurring in dystrophic and oligotrophic lakes and pools. The presence of these heavily silicified *Aulacoseira* suggests an increase in water turbulence and silica content, as well as low light conditions (Reynolds, 1984; Kilman et al., 1996). Higher productivity was also evidenced in the highland's sequence of Laguna de la Roya by a rise in total diatom accumulation rates and the increase in planktonic diatoms from 14.7 to ca. 12.7 cal ka BP (Muñoz Sobrino et al., 2013).

The lower content of most detrital-related elements and the higher organic contents also reflect the retreat of the Tera glacier from the lake basin into the high altitude areas of the watershed, and the onset of lake sediment dynamics with reduced glacier influence during Greenland interstadial GI-1c (Fig. 6). Lower sediment input to the lake is consisten with a denser vegetation cover and lower soil erosion. Regional pollen sequence in Laguna de las Sanguijuelas registered a decrease in herbaceous steppe vegetation and an increase in Betula (<10%) and Quercus robur-type (20%) between ca 14.0-13.6 cla ka BP. However the pollen sequence of Lleguna refletcs a decline in the values for Pinus pollen (90-40%) and a new increase in Betula pollen (15%) between ca 14.0-13.4 cal ka BP related to a retreat of woodlands to the southern valleys as a result of the environmental deterioration leading into

the Younger Dryas (Muñoz Sobrino et al., 2004, 2007). La Roya sequence shows the development of pine and oak woodlands from 14.5-12.5 cal ka BP, and two cool stages characterized by decreases of Pinus and increases in juniper pollen, at ca 13.6-13.3 (Intra-Allerød Cold Period-I, GI-1c2) and 13.3-12.9 cal ka BP (Intra-Allerød Cold Period-II, GI-1b). These two short events are also documented by the decrease in chironomid-inferred July temperatures (Muñoz Sobrino et al., 2013). In the Sanabria sequence, the clastic layer (base of subunit 2B, ca 13.0 cal ka BP) (Figs. 5, 6 and 9), could reflect a cooler episode and small glacial advance at the end of GI-1 and during GS-1 (13.0-12.4 cal ka BP, see below), synchronous with a regressive vegetation cover (a decline in total tree pollen of <10% and an increase in *Gramineae* at 13.6-12.8 cal ka BP in Laguna de las Sanguijuelas, Muñoz Sobrino et al., 2004, 2007) and increased soil erosion.

The sedimentological and geochemical Sanabria record does not show evidences of a cooling trend along GI-1 as observed in Greenland ice cores and documented in pollen sequences from other nearby lakes located in the oceanic highlands from NW Iberia (Lagoa de Marinho, Ramil-Rego et al, 1998; Lagoa de Lucenza, Muñoz Sobrino et al., 2001), and in chironomid reconstructed temperatures in Laguna La Roya (Muñoz Sobrino et al., 2013). The depositional and limnological dynamics of Lake Sanabria seem more consistent with a warming trend, similarly to other sites in northern Spain (Charco da Candieira, van der Knaap and van Leeuwen, 1997; Pindal cave, Moreno et al, 2010b; Estanya Lake, Morellón et al., 2009). The different sensitivity of the biological and geochemical proxies to seasonality may be behind the observed contradictions among records. Other southern western Mediterranean records show the same warming and increase in humidity during this interval (Genty et al., 2006; Combourieu Nebout et al., 2009; Rodrigo-Gámiz et al., 2011). A persistent negative "NAO-like" condition during the Bølling-Allerød period, with southward migration of the Westerlies, has been postulated to explain the increase in humidity (Rodrigo-Gámiz et al., 2011)

associated to the re-activation of the North Atlantic Thermohaline circulation and warmer North Atlantic SST (Sea Surface Temperature) (Martrat et al., 2007; Clark et al., 2012).

5.3. A glacier reactivation at 13.0 cal ka BP (GS-1 / Younger Dryas-YD)

Deposition of a clastic layer (facies E) with lower organic (TOC=3%, and TN=0.3%, C/N=13) and biogenic silica (2.7%) contents associated to higher K, Si/Ti, Sr/Ti and $\delta^{13}C_{org}$ values (ca -26‰) at 13.0 cal ka BP (onset of subunit 2B) is a conspicuous event in Sanabria Lake deglaciation evolution, and is interpreted as a reactivation of the Tera glacier (Figs. 5, 6 and 9). This glacial re-advance occurred, within age model uncertainties, at the onset of GS-1 (12,850 cal yr BP; Lowe et al., 2008) and would be consistent with other glacier advances in the Alps (Ivy-Ochs et al., 2009) and Pyrenees (González-Sampériz et al., 2006).

After sedimentation of this coarse clastic layer, the GS-1 (YD) in the Sanabria sequence shows a double structure. A first stage (subunit 2B, 12.9 to 12.4 cal ka BP) with deposition of fine organic silts (facies E, Table 2) with high MS values suggests the glacial influence in the lake was still significant (Figs. 5, 6 and 9). Diatom assemblages show an increase in *A. subborealis* and a decrease in *A. valida* (Fig. 8). *A. subborealis* seems to be better adapted to low-light, turbid environments with good water mixing conditions (Reynolds, 2006; Clegg et al., 2007). Pollen sequences reveal a complex vegetation pattern: landscape around Laguna de las Sanguijuelas was characterized by *Artemisia–Gramineae* before 12.4 cal ka BP, whereas in Lleguna high percentages (>35%) of *Quercus* were recorded between 13.2 and 12.0 cal ka BP (Muñoz Sobrino et al., 2004, 2007), and pine and oak woodlands developed in the highlands (Laguna de La Roya) before 12.5 cal ka BP (Muñoz Sobrino et al., 2013). The different composition of synchronous pollen zones is explained by variable impact of factors like altitude, orientation and rain shadow (Muñoz Sobrino et al., 2004, 2007, 2013). In particular, in Sanabria, the rain shadow effect in the leeward lowlands is strong, causing

higher rainfall from the Atlantic fronts in the Sierra Segundera mountains, and drier conditions and higher temperatures on the eastern slopes (Muñoz Sobrino et al., 2004). Paired hydrological and palynological oscillations in Lleguna (Muñoz Sobrino et al. 2004, 2007) are coherent with local vegetation changes associated to higher lake levels between 13.2 and 12.0 cal ka BP followed by a period of decreasing water levels. The sedimentation pattern in Sanabria sequence also suggests that during this period, melting of snow accumulated on the highlands may have fed the lake, minimizing seasonal variations.

A second stage (subunit 2A, 12.4-11.7 cal ka BP) with the deposition of facies D (Table 2) was characterized by a decrease in organic content and MS values and the highest BioSi content (Figs. 5, 6 and 9), and interpreted as lower glacial influence in the lake. The diatom concentration, dominated by *A. subborealis*, reached the highest values in the whole sequence (Fig. 8) marking the onset of nutrient enrichment in oligotrophic systems (Sabater and Haworth, 1995). The highest Si/Ti and BioSi values are indicative of the rapid development of diatoms. Higher concentrations of As and organic matter content (BioSi) suggest more frequent suboxic conditions in the sediments (Dean, 1993; Bradbury et al., 2004) (Fig. 6). All these indicators suggest a higher lacustrine phytoplankton contribution to the lake organic matter budget and increased productivity (Figs. 5 and 8). Contrarily, the total diatom accumulation rates in the highlands (Laguna de la Roya) decreased during the YD as an effect of the shortening of the ice-free season (Muñoz Sobrino et al., 2013). Decreases in MS and clastic-related elements (K, Ti) are consistent with lower run-off and sediment delivery to the lake (Fig. 6 and 9). These inferences are supported by pollen evidence of tree recovery (*Pinus*=70%) between ca 12.4-11.8 cal ka BP in Laguna de las Sanguijuelas, and coincide with a stage of *Pinus* maxima (>60%) recorded in Lleguna at 12.0–11.6 cal ka BP (Muñoz Sobrino et al., 2004, 2007). Laguna de la Roya reveals a more open vegetation at 12.5-11.8 cal

ka PB, and a 2ºC cooling in chironomid-inferred summer temperatures during the GS-1 (Muñoz Sobrino et al., 2013).

Although a general trend towards colder temperatures and aridity has been recorded from northern Iberia during the YD (Santos et al., 2000; Muñoz Sobrino et al., 2001; González-Samperiz et al., 2006; Morellón et al., 2009; Moreno et al., 2010b, 2011; Morales-Molino and García-Antón, 2014) (Fig. 1B), the double structure of the YD in the Sanabria sequence is coherent with reconstructions in the southwest (van de Knaap and van Leeuwen, 1997; Rodrigues et al., 2010) and northwest (Leroy et al., 2000; Bos, 2001; Bakke et al., 2009) Europe, and with simulation experiments (Isarin et al., 1998, Alley, 2000; Lowe et al., 2008). Both paleodata and models indicate a cold period during the onset of YD, followed by less cool conditions, related with latitudinal shifts and intensity of the Westerlies (Bakke et al., 2009).

5.4. The onset of the Holocene (11.7-10.1 cal ka BP)

The transition to the Holocene (11.7-10.1 cal ka BP) is recorded in the upper 10 cm of subunit 2A (facies A, Table 2) with slightly increasing organic matter content and higher values of BioSi, both indicative of higher bioproductivity (Figs. 5 and 6). There are no clear sedimentological or geochemical evidences of the 11.2 cal ka BP cooling event, identified in nearby sequences by a decrease in regional woodland cover (Muñoz Sobrino et al., 2004, 2007, 2013). However, deposition of organic silts with more abundant plant remains and higher MS (facies G, subunit 1E) at about 11.2 cal ka BP underlines the definitive change in Sanabria lake dynamics towards limited glacial influence in a more forested watershed at that time (Figs. 5 and 6). Pollen sequences from Lleguna, Laguna de las Sanguijuelas, and Laguna de la Roya show an increase in tree pollen taxa between 11.8 and 10.2 cal ka BP (Muñoz Sobrino et al., 2004, 2007, 2013). The higher TOC content, along the C/N atomic

ratio and δ^{13}Corg values show that the sediment organic matter is a mixture of lake and land material, with higher relative proportion of algal organic matter (lower δ^{13}Corg and C/N, and higher BioSi content) in subunit 2A (Lateglacial and the onset of Holocene) and higher proportions of land-derived organic matter in unit 1 (Holocene) (Fig. 5). The diatom community is dominated by *A. subborealis* (although decreasing upcore), with small but increasing percentages of *T. flocculosa* var. *linearis* (Fig. 8). The dominance of *A. subborealis* would indicate higher lake-levels (and correspondingly effective moisture, i.e. higher precipitation, run-off variability and snowmelt), since this species is a common planktonic diatom associated with relatively high turbulent waters (Rühland and Smol, 2005; Harris et al., 2006). The small increases in *T. flocculosa* var. *linearis,* and other benthic diatoms as *S. angusta,* could be related to higher turbulence caused by stronger winds, mobilizing benthic diatoms into the plankton, rather than to a lake level decrease. Species as *Surirella* are heavily silicified diatoms common in littoral sediments, especially epipelic habitats. The presence of diatoms of different ecological groups (e.g. planktonic, epiphytic, epipelic…) in the samples of this period would indicate preferential transport, high diversity of ecological niches or strong seasonality (wet winters and dry summers). In the highlands, an increase in productivity (*Aulacoseira alpigena*, 20-60%) from 11.7 to ca 11.5 cal ka BP followed by a decreasing trend to ca 10.5 cal ka BP (*A. alpigena*, 60-30%) was recorded in Laguna de la Roya (Muñoz Sobrino et al., 2013).

5.5. The Early Holocene (10.1-6.8 cal ka BP)

Considering sediment input, two main periods can be differentiated in Sanabria along the Early Holocene, (1) a first period (10.1-8.2 cal ka BP, subunit 1C) with distinctive coarse-clastic layers that mark higher sediment input into the lake during large flooding events (facies Ha, at 10.1 and 8.4), and (2) a second period (8.2-6.8 cal ka BP) with a clear reduction

in the frequency of clastic layers suggesting less extreme hydrological events, and only one main coarse-clastic layer at 7.5 cal ka BP (Figs 5 and 6). Lleguna sequence also showed a first flooded stage at ca 8.4 cal ka BP followed by lower water levels at ca 8.2 cal ka BP and a later recovery phase. In Laguna de las Sanguijuelas a probable depositional hiatus has been proposed at this time (Muñoz Sobrino et al., 2004). Negative $\delta^{13}C_{org}$ and positive BioSi excursions within this period indicate an increase in productivity that occurred after the high runoff events; a mechanism previously illustrated by a twenty-years monitoring survey in the lake (Giralt et al., 2011).

This hydrological pattern during the Early Holocene with a first humid stage prior to ca 8 cal ka BP and decreased precipitation and more stable conditions during the second part is registered in other continental records in Northern Iberian Peninsula (Quintanar de la Sierra, Peñalba et al., 1997; Laguna Lucenza and Fraga, Santos et al., 2000; El Portalet, González-Sampériz et al., 2006; Roñanzas peatbog, Ortiz et al., 2010; Enol Lake, Moreno et al., 2011; Penido Vello peatbog, Schellekens et al., 2011) (Fig. 1B). Shallow marine core form the NW Iberian margin (Pena et al., 2010) showed a similar pattern: decreasing trend in $\delta^{13}C$ values of benthic foraminifera from 8.2 to 7.3 cal ka BP resulting from increased continental runoff (more rainfall associated with the presence of the storm tracks over NW Iberia), followed by positive $\delta^{13}C$ excursions between ca 7.3-6.5 cal ka BP (less rainfall due to a southward shift in the main position of the storm tracks) (Fig. 9). Interestingly, there is a clear Atlantic versus Mediterranean variability, with some NE Iberian sequences indicating a late onset of Holocene humid conditions (Lake Estanya, Morellón et al., 2009) and even an opposite early Holocene paleohydrological evolution (e.g. in the central Pyrenees, Basa de la Mora, Pérez-Sanz et al., 2013). Likely, these dissimilarities are associated to regional variability and asynchronous responses to the precipitation gradient rather than to uncertainties in the chronological models. At a more regional scale, phases of increasing humidity around 10.2,

8.2 and 7.3 ka cal BP have been identified in Lake Saint-Point, France (Magny et al., 2013a), Lake Accesa, Italy (Magny et al., 2012; 2013b) and Lake Ledro, Italy (Magny et al. 2007, 2013b; Vannière et al., 2013; Simonneau et al., 2013b) (Figs 1A and B, 9).

Abrupt Early Holocene climate variability has been documented in numerous records in the North Atlantic region, associated to cooling events caused by abrupt changes in the atmospheric circulation, and with ice rafted in the North Atlantic (Bond et al., 1997) (Fig. 9). The Sanabria flooding events at 10.1, 8.4 and 7.5 cal ka BP could tentatively correlate with a decrease in tree pollen (85-70%, 80-60% and 85-75% respectively) detected in the nearby Lleguna but no clearly apparent in the Laguna de las Sanguijuelas (Muñoz Sobrino et al., 2004, 2007), and may correspond to the short 10.2, 8.4 and 7.4 cooling events (Bond et al., 1997) (Fig. 9). Molecular vegetation markers document a humid stage around 7.6-7.2 cal ka BP in Roñanzas (Ortiz et al., 2010) and in Penido Vello (Schellekens et al., 2011) peatbogs.

The most prominent of the Early Holocene abrupt events at 8.2 ka BP (Bond event 5) was caused by changes in ice sheet extent and meltwater releases into the North Atlantic (Alley et al., 1997; Mayewski et al., 2004). In the context of the IP, the 8.2 ka BP shows large regional variability in terms of timing and impacts, showing different intensities for various climate-sensitive locations in NW Iberia. In the Sanabria sequence, this event corresponds to the deposition of a thin clastic layer and marks the beginning of a climatic deterioration (Fig. 9). In the nearby Lleguna and Laguna de las Sanguijuelas (Allen et al., 1996; Muñoz Sobrino et al., 2004, 2007), and in other regional (La Roya, Allen et al., 1996) and extrarregional pollen sequences (Lucenza, Santos et al., 2000; Muñoz Sobrino et al., 2001) the 8.2 event is described by a generalized reduction of the total tree pollen, particularly deciduous *Quercus*. Pollen evidences from Lagoa de Marinho and Chan do Lamoso (NW Iberia) (Ramil-Rego et al., 1998), suggest that hydro-hygrophilous vegetation enhanced during a cooler and moister

8.2 event. In Northeastern IP, this event has been also associated with arid conditions González-Sampériz et al., 2006; Morellón et al., 2009; Moreno et al., 2011), and with a rapid cooling in the Portuguese Margin (Rodrigues et al., 2009).

5.6. The Mid Holocene (6.8 – 4.8 cal ka BP)

The Mid Holocene in the Sanabria record (subunit 1D, 6.8-4.8 cal ka BP) is characterized by sedimentation of organic rich silts with relatively high BioSi content, the lowest MS values (facies F, Table 2) and absence of facies G (Figs. 5 and 6). *A. subborealis* and *T. flocculosa* var. *linearis* are the most abundant diatom species, but relatively higher abundance of tychoplanktonic *T. flocculosa* var. *linearis* may reflect an expansion of littoral habitats, more conducive for macrophytes development (Douglas and Smol, 1995; Reavie and Smol, 1997) (Fig. 8). The abundance of both planktonic and benthic assemblages could indicate relatively stable conditions favoring benthic diatom blooms, since periods of higher stratification and stability could decrease the development of *Aulacoseira spp.* (Rühland and Smol, 2005; Harris et al., 2006). The diatom assemblages and the chrysophyte cyst to diatom frustules ratio in Lagoa Grande (Galicia, NW Spain) ca. 6,000 BP have been interpreted as decreased productivity, cold water and possibly shallower conditions (Leira, 2005).

Sedimentological, palynological and diatom data suggest that the Mid Holocene in NW Iberia was a warmer period than before, marked by reduced rainfall and lower sediment input into the lake associated with a denser catchment vegetation cover (Figs. 5, 8 and 9). In the nearby Lleguna and Laguna de las Sanguijuelas the tree pollen remained high (ca 90%) with mixed pine/oak formations, and increasing warmth-demanding taxa (Muñoz Sobrino et al., 2004). Although some sites in northern Iberia show moister mid-Holocene phases – e.g., 7500–4000 cal BP, Puerto de los Tornos peatbog's pollen sequence (Muñoz Sobrino et al., 2009), most regional lake records show evidences of increased aridity during the Mid Holocene (Laguna

Lucenza and Fraga sequences, Santos et al., 2000; Roñanzas peatbog, Ortiz et al., 2010; Enol Lake, Moreno et al., 2011). Also, a recent reconstruction of precipitation in NW Iberia derived from growth rates of 11 stalagmites shows a sharp decrease of precipitation after 6 cal ka BP (Stoll et al., 2013). The mid-Holocene moisture availability decrease has been explained as changes in mid latitudes associated to insolation decrease conducive to marked positive NAO-like mode in western Mediterranean areas, although the detailed mechanisms and teleconnections remain elusive (Gladstone et al., 2005; Wanner et al., 2008; Magny et al., 2013b).

Within this relatively arid Mid Holocene, short phases of increased fluvial input were detected in the Sanabria sequence by mm-thick clastic layers at 6.2 and 5.7-5.6 cal ka BP. Comparable inundation and recovery phases have been recognized in the nearby Lleguna (Muñoz-Sobrino et al., 2004). Many regional records show short periods of higher precipitation or hydrological balance during the Mid Holocene. In the central and eastern Cantabrian Mountains humid events were recorded by biomarker analyses in Roñanzas peatbog at ca 6.5 cal ka BP and 5.9-5.2 cal ka BP (Ortiz et al, 2010) and ca 6.1-4.9 BP in Penido Vello peatbog (Schellekens et al., 2011). Marine data also recorded humid phases ca 6.3 cal ka BP in NW Iberia (Pena et al., 2010), and at 5.4 cal ka BP in SW Iberia (Rodrigues et al., 2009). A phase of aeolian activity recorded in the Portuguese coast at 5.6 ka is explained as enhanced Westerlies during prolonged negative NAO-mode (Costas et al., 2012). At a global scale, short phases of increasing humidity around 6.2, 5.8–5.3 cal ka BP occurred in some North-central Mediterranean sites (Lake Saint-Point, France; Magny et al., 2013a) and west central European (Lake Accesa, Italy; Magny et al. 2013b and Lake Ledro, Italy; Magny et al. 2013b; Vannière et al., 2013) regions (Fig. 9).

Particularly, the 5.7-5.6 Sanabria flood event could be related to the cool event at 5.4 cal ka BP (Bond Event 4) (Bond et al., 1997) (Fig. 9) and the worldwide cooling event resulted from complex interactions between changes in orbital forcing, ocean circulation and solar activity (Magny et al., 2006).

5.7. The Late Holocene (4.8 – 1.5 cal ka BP)

Both sedimentological and geochemical data mark two main periods in Sanabria sequence along the Late Holocene: (1) A first stage (subunit 1C, 4.8-3.3 cal ka BP) characterized by higher Ti and K values, a small increase in MS values and more frequent clastic facies G (4.2, 3.7 and 3.3 cal ka BP) and Ha (4.6 cal ka BP) than before, (2) A second stage (subunit 1B, 3.3-1.5 cal ka BP) characterized by fewer discrete clastic layers (3.1, 2.5, 2.0 and 1.5 cal ka BP) and facies Ha (2.7 cal ka BP) but with relatively high MS values suggesting increased sediment delivery to the lake not only during flooding episodes (Figs. 5 and 6). The $\delta^{13}C_{org}$ positive excursions at 4.6, 3.1 and 2.0 cal ka BP correlate with generally higher C/N values, lower BioSi concentration, coarser sediments, high Si, K, Fe, Ti contents and high MS values, suggesting a greater influence of allochthonous organic matter, transported by the Tera River.

Local sequences from Sanabria Lake (Luque, 2003; Julià et al., 2007) show relatively low percentages of arboreal pollen (42-50%), dominated by *Quercus*, and higher percentages of herbaceous pollen (38-45%) and aquatics (17-24%) and abundant *Cerealia*-type pollen before ca 1500 cal yr BP. Regional forest retreat in northwest Iberia since ca 4000 cal. BP is due to a combination of human impact and climatic factors (cold phases) (Muñoz Sobrino et al., 2009). Anthropogenic impact (e.g. forest burning for pastures or agriculture) has been particularly intense since 3 cal ka (Allen et al., 1996; Muñoz Sobrino et al., 2001, 2004; Leira and Santos, 2002). The general increase in MS after 3.3 cal ka BP could reflect this intense impact in the

landscape (Fig. 9). However, the Roman settlement in the area is not clearly translated into increased sediment delivery to the lake (Fig. 6 and 9).

The Sanabria diatom assemblage was dominated by the planktonic *A. subborealis* (60%) except during the 3.8-3.2 cal ka BP interval, when tychoplanktonic flora (*T. flocculosa* var. *linearis and T. flocculosa* var. *flocculosa)* strongly increased (60% and 10% respectively) and represents one of the most significant changes in the diatom communities during the Holocene (Figs. 8 and 9). Although the correspondence between higher tychoplanktonic diatom content and more clastic layers during this period could suggest increased fluvial activity as responsible for a higher input of diatoms from benthic environments, we do not find a similar relationship during other periods of increased clastic input to the lake. So, we favor limnological changes, such as lowering of lake levels, as responsible for the development of more benthic habitats. This relatively arid phase in Sanabria could correspond to a drier phase interpreted in Lagoa Grande (Leira, 2005) and in the Galician shelf (Bernárdez et al., 2008; Pena et al., 2010; Muñoz Sobrino et al., 2012).

Correlation of this short–term Late Holocene climate and environmental variability in Sanabria with other regional records is not straightforward, likely because of regional variability and dating uncertainties. Similar increases in humidity during the late Holocene was interpreted in Roñanzas peatbog (Ortiz et al., 2010) and Enol Lake (Moreno et al., 2011). However, dry conditions occurred in Galician offshore (NW Spain) up to 3.3 cal ka BP - deep sites (4.7-3.3 cal ka BP, González Álvarez et al., 2005) and shallower sites (4.0-3.4 cal ka BP, Bernárdez et al., 2008) – and were followed by more humid conditions between 3.3 and 1.7 cal ka BP (Diz et al., 2002, Lebreiro et al., 2006; Bernárdez et al., 2008). Benthic foraminiferal stable isotopes in the Ría de Muros (Pena et al., 2010) suggest rapid events of less rainfall at 3,700-2,900 and at 1,800 cal yr BP. And dinocyst records in Ría de Vigo

(Muñoz Sobrino et al., 2012) show short cold and dry events at about 4.6-4.3 and 3.8-3.6 cal ka BP, intercalated with warmer and wetter periods from 4.3 to 3.8 cal ka BP and from 3.6 to 3.2 cal ka BP.

The hydrological variability interpreted from the Sanabria Lake clastic layers (4.6, 4.2, 3.7 3.3, 3.1, 2.7, 2.5, 2.0 and 1.5 cal ka BP) has been also documented by biomarker content in Penido Vello peatbog (2300 BC, 1505–1260 BC, 1055–960 BC, 640–440 BC, 260–140 BC, 45 BC–15 AD, 135 AD, 190–215 AD, 270–385 AD, Schellekens et al., 2011). At European scale, the same two Late Holocene hydrological stages have been identified in Lake Ledro (northern Italy): increase of the mean flood frequency from 4.2 to 3.1 cal ka BP, followed by a progressive decrease of flood deposits from 3.1 to 1.2 cal. ka BP (Simonneau et al., 2013b). Phases of increasing humidity, inferred by the predominance of terrestrial organic supply, occurred at around 4.8, 4.4–3.8, 3.3, 2.7-2.3, 1.7, 1.2 cal ka in North-central Mediterranean (Lake Saint-Point, France; Magny et al., 2013a; Lake Majeur, France; Simonneau et al., 2013a) and west central European (Accesa Lake, Italy, Magny et al. 2013b and Ledro lake, Italy; Magny et al. 2013b, Vannière et al., 2013, Simonneau et al., 2013b) (Fig. 9). In these regions, Late Holocene flood events have been attributed to positive synergies between cold climatic oscillations and human-induced soil destabilization and erosion.

The main clastic layers at 4.6 and 2.7 ka BP in the Sanabria sequence could represent the Holocene cooling Bond events 3 and 2 (Bond et al., 1997) (Fig. 9). Again, more frequent NAO negative-like periods have been postulated as the main driver for periods of increased precipitation in NW Spain (Lebreiro et al., 2006; Bernárdez et al., 2008, Muñoz Sobrino et al., 2012). The 4.6 clastic layer marked a climatic change between a dry Mid Holocene and humid Late Holocene, and has been considered as the onset of dominant negative NAO-mode and a southward migration of westerlies, and linked to a non-linear response of the climate system

to the gradual decrease in insolation in addition to other key seasonal and interhemispherical changes in insolation (Zhao et al., 2010, Magny et al., 2013b; Vannière et al., 2103).

5.8. The last 1.5 cal yr BP.

During the last millennium the absence of discrete clastic layers parallels a higher sediment delivery to the lake as indicated by MS and geochemical indicators (subunit 1A) (Figs. 5, 6 and 9). This diffuse clastic input to the lake could be associated to a combination of climate and human forcing. Negative $\delta^{13}C_{org}$ excursions at 1.3 and 1.2 cal ka BP are not associated to clastic layers, and they are rather more likely due to changes in productivity or trophic state. The dominance of planktonic diatom *A. subborealis* is indicative of relatively humid conditions during the Dark Ages (AD 500-900) (Fig. 8). Julià et al. (2007) interpreted warmer conditions and higher effective runoff between 440 and 650 AD followed by a period of more regular rainfall regimen and a decrease in temperatures from 650 to 950 AD. Abundant cerealia-type pollen marked the foundation of the San Martín de Castañeda Monastery in the 6th century AD (Julià et al., 2007). Most terrestrial Iberian records show high lake levels during the Roman Period (AD 0-500) – Dark Ages (AD 500-900) (Morellón et al., 2009; Ortiz et al., 2010; Schellekens et al., 2011; Corella et al., 2013). However, marine records offshore Galicia (NW IP) show a dry and cold period between 1.7 and 1.2 cal ka BP, and an increase in the precipitation since 1.2 cal. ka BP interpreted as dominant NAO negative mode (Bernárdez et al., 2008).

Our set of cores does not contain the complete Medieval Climate Anomaly (MCA) interval (900-1300 AD). The clastic layers during the 950-850 cal yr BP period (top of the long core) could be a reflection of increased human pressure in the watershed during the 9th–10th centuries brought by new settlements in the area (Luque and Julià, 2002; Julià et al., 2007) and still wet conditions (Fig. 6 and 9). Sanabria short cores (Luque, 2003; Julià et al., 2007) show

higher lake productivity and a decrease in arboreal pollen percentages during the onset of the MCA up to until ca 1100 AD. Biomarker content from Penido Vello peatbog reveals a humid stage at 930-1045 AD followed by drier conditions (AD 1085-1385) (Schellekens et al., 2011). Most northern continental Iberian records (peatbog and lacustrine archives) show more arid conditions during the MCA (see Moreno et al., 2012b and reference therein) potentially associated with more frequent NAO positive phases (Trouet et al., 2009; Moreno et al., 2012b). In the marine realm, however, the MCA hydrological signature is not unequivocal: shallow marine records from NW Iberian Margin, Ría de Muros (Lebreiro et al., 2006; Pena et al., 2010) and the Ría de Vigo (Desprat et al., 2003) show warmer and humid conditions during AD 800-1300, whereas the Tagus prodelta site (SW Iberian Margin) (Abrantes et al., 2005; Lebreiro et al., 2006) suggests opposite patterns. Despite of this latitudinal variability, northwestern Iberian continental records are consistent with a dominant positive NAO mode during the MCA, and with northward-shifted westerly winds (Moreno et al., 2012b). Discrepancies in moisture evolution between NW and SW Iberian regions during Medieval Climate Anomaly - Little Ice Age (MCA/LIA) transition have been explained as a reflection of different geographical location and impact of NAO dynamics (Lebreiro et al., 2006). At European scale, the transition MCA/LIA show a long-term trend from low to high flood frequency; global forcing factors such as insolation variability could have been a significant driving force in hydrological dynamics (Vannière et al., 2013; Simoneau et al., 2013a,b; Corella et al., 2013). Interestingly, although human impact (e.g deforestation, fires and farming activities) in the watershed is a main factor generating sediment to be delivered to Sanabria Lake, and in spite of the intense human activities during medieval times in the Sanabria watershed, discrete clastic layers associated to floods were more frequent during Roman and Medieval times than during the LIA.

The short cores (SAN07-1M and 2M) illustrate a large variability of Sanabria Lake dynamics from AD ca 1520-2005 (Fig. 7). The first phases of the LIA are characterized in the Sanabria 2M core by deposition of organic-rich silts with relatively high BioSi (5%) but lower diatom concentration (AD ca 1520-1600) followed by more clastic-rich sediments particularly between AD ca 1670-1760 (Fig. 7). Within the age-depth model errors, the 2M more clastic interval correlates with the period of higher siliciclastic input (wet phase), lower arboreal pollen content and presence of cultivated taxa between ca 1500-1700 AD identified by Luque (2003), Juliá and Luque (2006) and Juliá et al. (2007). *A. subborealis* percentages also followed a decreasing trend (60-45%) parallel to the increasing values of *A. minutissimum* (5-15%) and *F. arcus* (5-10%). Depleted diatom productivity, as indicated by the decrease in total and planktonic diatom accumulation rates could suggest a dominance of periphytic habitats and also a prolonged ice cover of the lake. From AD ca. 1760 till 1950 BioSi, diatom concentration, TOC and TN values increased. *A. subborealis* increased (45-60%) whereas *F. arcus* decreased (5%) as lake productivity recovered (Fig. 7). *Cyclotella stelligera* appears for the first time (0.6%). Similar increasing trends in lake productivity were documented in other Sanabria cores (Luque and Julià, 2002; Luque, 2003; Julià and Luque, 2006; Julià et al., 2007). All these indicators point to a climatic improvement consistent with the forest recovery detected after ca 1600 AD (Julià et al., 2007) (Fig. 7).

In the Iberian Peninsula, the LIA is characterized by general cooling, more humid conditions and increased frequency of weather extremes, although with large hydrological variability (Desprat et al., 2003; Abrantes et al. 2005, 2011; Lebreiro et al., 2006, Bernárdez et al., 2008; Moreno et al., 2008; Morellón et al., 2009; Ortiz et al., 2010; Schellekens et al., 2011; Moreno et al., 2012b). A bipartition can be also identified in the Pyrenees with a 1600-1800 AD period characterized by lower temperatures and wetter conditions than earlier (Saz Sánchez 2003, Corella et al., 2012; Morellón et al., 2011, 2012; Moreno et al., 2012b). At European scale,

higher frequency of clastic layers (hydrological events) at AD 1500–1850 reveals further consistency with negative NAO index (wetter conditions) and with solar minima irradiance (colder climate) (Trouet et al., 2009, Simonneau et al., 2013a).

The prominent clastic, fining-upward layer (facies Hb) and the expansion of *C. stelligera,* represents the dam breach deposit caused by the Tera River flash flood after the dam collapsed in AD 1959 (Fig. 7), previously documented in short cores by Luque and Julià (2002), Luque (2003), Julià and Luque (2006) and Giralt et al. (2011). Sanabria Lake experienced a catastrophic flood during the night of January 9th, 1959 when the Vega de Tera Dam (altitude 1503 m a.s.l., 8 km north-west from Ribadelago village) collapsed, causing a flood (>16.000 $m^{3}{\cdot}s^{-1}$, ca. 8 million m^3 of water), which partially destroyed the village of Ribadelago, killed 172 inhabitants and the water level of the Sanabria Lake raised around 2.3 m (García Diez, 2003). Considering the sedimentological signatures, no similar flooding had occurred in the lake since the Early Holocene. Interestingly, the Tera Dam collapse in 1959 marked a significant change in the lake dynamics, but the recovery of the Sanabria Lake system after the Dam breach was relatively rapid. The upper lake sediments show high TOC content, low C/N ratio, a negative $\delta^{13}C_{org}$ (from -26 to -28‰) excursion, and higher BioSi concentration, all indicative of higher contribution of autochthonous OM sources to the carbon budget in the Lake, lower detrital input, and also an increase in bioproductivity (Fig. 7). Pollen data from AD 1960 onwards indicate a relatively forested landscape dominated by native deciduous oak and birch (Julià et al., 2007). A large change occurred in the diatom assemblages with the appearance of *C. stelligera*, a decrease in planktonic *A. subborealis* and an increase of benthic diatoms (*Fragilaria, Pinnularia, Staurosira*) after the 1960s (Fig. 7). In temperate lakes, *Aulacoseira* species are common in the water column in early spring due to their low light and high water turbulence requirements (Reynolds 1984, Kilman et al,. 1996), followed by *Cyclotella, Fragilaria* and *Tabellaria* spp. in the spring maximum (Wetzel, 1983). Turbulent

conditions are important in particular for *Aulacoseira* because of its rapid sinking rate resulting from the high silica content (Round et al., 1990). Rise in various *Cyclotella* taxa have been linked to climate change throughout lakes in the Canadian arctic (Karst-Riddoch et al., 2005) as well as in temperate regions (Wolin and Stoermer, 2005). The changes in the duration of the overturns and summer stratification may have favored the growth of small *Cyclotella* species through the increased nutrient availability from the hypolimnion during the autumn mixing. Thus, changes in water and nutrient input to the lake, and temperature could be responsible for the observed increased in *C. stelligera,* paralleled by a relative decrease in *A. subborealis* in the 70's and 80's. Hydrological changes due to the construction of several dams in the Tera River could have also been a main factor since they reduce flushing rate, produce nutrient enrichment and cause deterioration of littoral environments through drawdown. The limnological impact of dams and hydropower activities in a lacustrine environment has been documented in Lake Majeur (Pyrenees, France) revealing modifications in the natural lake sedimentary dynamic of the lake, changes in the trophic state and in the source of sedimentary organic matter (Simonneau, et al., 2013a). Although Sanabria Lake area was declared a Natural Park in AD 1978, human impact caused by tourism (sewage and wastewater) and increased fires in the watershed from the 1990's had likely an impact on sediment and nutrient delivery to the lake. Nutrient enrichment loading through different human activities strongly influences the phytoplankton growth (de Hoyos and Comín, 1999) and provides a plausible explanation for recent changes in $\delta^{13}C$ values.

6. CONCLUSIONS

A sedimentological, geochemical and biological study of a set of sediment cores from Sanabria Lake constrained by a robust ^{14}C chronology, provides the first multiproxy-based reconstruction of the timing and dynamics of the last deglaciation and the Holocene climate variability in the NW Iberian Peninsula. The timing of main climatic phases is in agreement

with oscillations described in Greenland ice cores (Rasmussen et al., 2006; Vinther et al., 2006) and in other marine and terrestrial Western European sequences (Fletcher and Sánchez Goñi, 2008; Lowe et al., 2008; Combourieu Nebout et al., 2009). The maximum extent of the Tera glacier occurred before the global LGM, similarly to other alpine glaciers in southern Europe's mountains. After a rapid retreat during the Greenland Interstadial GI-1e (Bølling, 14.6 cal ka BP), and a short glacier re-advance (14.4-14.2 cal ka BP, likely corresponding to GI-1d), the Tera glacier retreated from the Sanabria Lake Basin at 13.9 cal ka BP during moister and warmer GI-1c. The warming trend along GI-1 interpreted in Sanabria and other Iberian records contrasts with the cooling trend documented in Greenland ice cores, and further illustrates a different behavior during deglaciation in high and intermediate latitudes. After a final glacier reactivation phase between ca 13.0-12.4 ka, synchronously to the GS-1 (Younger Dryas interval), glaciers disappeared from the Sanabria watershed in the Early Holocene.

Increasing temperatures and lake bioproductivity occurred at the onset of the Holocene (11.7 – 10.1 cal ka BP), followed by a humid period (10.1-8.2 cal ka BP) with higher sediment delivery to the lake. The 8.2 to 6.8 cal ka BP period is a transitional stage, with the onset of a decreasing humidity trend that culminated with a drier Mid Holocene (6.8-4.8 cal ka BP) and continued during the Late Holocene, although punctuated by a significant humid phase from 4.8 to 3.3 cal ka BP, and a smaller one during the LIA. Episodes of increased river input detected in Sanabria sediments (10.1, 8.4, 7.5, 6.2, 5.7-5.6, 4.6, 4.2, 3.7, 3.3, 3.1, 2.7, 2.5 and 2.0 cal ka BP) are in agreement with European records at similar latitudes and the RCC (Rapid Climate Change) intervals (Mayewski et al., 2004).

The Sanabria record demonstrates that hemispheric Holocene cooling events (e.g. 10.2, 8.4 and 7.5-7.0 ka cal BP) correspond in mid-latitudes and the Mediterranean region to humid

conditions, in response to strengthened Atlantic westerly jet. Although several atmospheric modes – the Scandinavian Pattern (SCA), the Eastern Atlantic (EA) and the Eastern Atlantic/Western Russia (EA/WR) the North Hemisphere Annular Mode (NAM) - explain some of the observed variability of the main synoptic weather types on Iberia, the North Atlantic Oscillation (NAO) represents the main mode of climate variability in the NW Iberian Peninsula during winter. Considering that similar climate forcings could have operated during the Holocene, although at different time-scales, positive NAO mode-like (decrease winter precipitation) would have prevailed during the mid part of the Holocene (since 8.2, but particularly between 6.8 and 4.8 cal ka BP) and negative NAO mode-like (maximum winter precipitation) during the early part of the Holocene (10.1-8.2 cal ka BP) and some phases of the late Holocene (4.8-3.3 cal ka BP and LIA).

7. ACKNOWLEDGEMENTS

Funding for this research has been provided by the Spanish Ministry of Economy and Competitiveness through the CALIBRE CGL2006-13327-C04-01/CLI and CONSOLIDER-GRACCIE CSD2007-00067 projects and by the Fundación Patrimonio Natural Castilla y León. M. Jambrina-Enríquez is supported by a PhD fellowship from Salamanca University (Spain). A. Moreno acknowledges the funding from the "Ramón y Cajal" postdoctoral program. We are grateful to Doug Schnurrenberger, Anders Noren and Mark Shapley (LRC, University of Minnesota) for the 2004 coring expedition. We thank Parque Natural Lago de Sanabria and Laboratorio Limnológico de Sanabria (Junta de Castilla y León) for logistic support. We are also grateful to the detailed criticisms and suggestions by two reviewers that greatly improved the manuscript.

8. REFERENCES

Abrantes, F., Lebreiro, S., Rodrigues, T., Gil, I., Bartels-Jónsdóttir, H., Oliveira, P., Kissel, C., Grimalt, J.O., 2005. Shallow marine sediment cores record climate variability and earthquake activity off Lisbon (Portugal) for the last 2,000 years. Quaternary. Sci. Rev. 24, 2477-2494.

Abrantes, F., Rodrigues, T., Montanari, B., Santos, C., Witt, L., Lopes, C., Voelker, A.H.L., 2011. Climate of the last millennium at the southern pole of the North Atlantic Oscillation: an inner-shelf sediment record of flooding and upwelling. Clim. Res. 48, 261–280.

Aldasoro, J.J., De Hoyos, C., Vega, J.C., 1991. El lago de Sanabria (Estudio Limnológico). Publicaciones Monográficas de la Red de Espacios Naturales de Castilla y León. Consejería de Medio Ambiente y Ordenación del Territorio. Dirección General del Medio Ambiente, Valladolid, Spain.

Allen, J.R.M., Huntley, B., Watts, W.A., 1996. The vegetation and climate of northwest Iberia over the last 14,000 yr. J. Quaternary Sci. 11, 125–147.

Alley, R.B., Mayewski, P.A., Sowers, T., Stuiver, M., Taylor, K.C., Clark, P.U., 1997. Holocene climatic instability: A prominent, widespread event 8200 years ago. Geology 25, 483-486.

Alley, R.B., 2000. The Younger Dryas cold interval as viewed from central Greenland. Quaternary Sci. Rev. 19, 213-226.

Atlas Agroclimático de Castilla y León- ITACYL-AEMET-. 2013. [http://atlas.itacyl.es].

Bakke, J., Lie, Ø., Heegaard, E., Dokken, T., Haug, G.H., Birks, H.H., Dulski, P., Nilsen, T., 2009. Rapid oceanic and atmospheric changes during the Younger Dryas cold period. Nature Geosci 2, 202–205.

Battarbee, R., 1986. Diatom analysis. In: Berglund, B.E. (Ed.), Handbook of Holocene Palaeocology and Palaeohydrology. Wiley, Chichester, pp. 527–570.

Battarbee, R.W., Carvalho, L., Jones, V.J,. Flower, R.J., Cameron, N.G., Bennion, H., Juggins, S., 2001. Diatoms. In: Last, W.M., Smol, J.P. (Eds.). Tracking Environmental Change Using Lake Sediments,Terrestrial, Algal, and Siliceous Indicators, vol. 3. Kluwer Academic Publishers: Dordrecht, The Netherlands, pp. 155–202.

Bernárdez, P., Prego, R., Francés, G., González-Álvarez, R., 2005. Opal content in the Ría de Vigo and Galician continental shelf: biogenic silica in the muddy fraction as an accurate paleoproductivity proxy. Cont. Shelf. Res. 25, 1249–1264.

Bernárdez, P., González-Álvarez, R., Francés, G., Prego, R., Bárcena, M.A., Romero, O.E., 2008. Late Holocene history of the rainfall in the NW Iberian peninsula—Evidence from a marine record. J. Marine Syst. 72, 366–382.

Blaauw, M., 2010. Methods and code for 'classical' age-modelling of radiocarbon sequences. Quaternary Geochronology 5: 512-518

Bond, G., Showers, W., Cheseby, M., Lotti, R., Almasi, P., de Menocal, P., Priore, P., Cullen, H., Hajdas, I., Bonani, G., 1997. Pervasive Millennial-Scale Cycle in North Atlantic Holocene and Glacial Climates. Science 278, 1257-1266.

Bos, J.A.A., 2001. Lateglacial and Early Holocene vegetation history of the northern Wetterau and the Amöneburger Basin (Hessen), central-west Germany. Rev. Palaeobot. Palyno. 115, 177-212.

Bradbury, J.P., Colman, S.M., Dean, W.E., 2004. Limnological and Climatic Environments at Upper Klamath Lake, Oregon during the past 45000 years. J. Paleolimnol. 31(2), 167-188.

Carrión, J.S., Fernández, S., González-Sampériz, P., Gil-Romera, G., Badal, E., Carrión-Marco, Y., López-Merino, L., López-Sáez, J.A., Fierro, E., Burjachs, F., 2010. Expected trends and surprises in the Lateglacial and Holocene vegetation history of the Iberian Peninsula and Balearic Islands. Rev Palaeobot Palynol 162, 458–475.

Chapron, E., Faïn, X., Magand, O., Charlet, L., Debret, M., Mélières, M.A., 2007. Reconstructing recent environmental changes from proglacial lake sediments in the Western Alps (Lake Blanc Huez, 2543 m a.s.l. Grandes Rousses Massif, France). Palaeogeogr Palaeoclimatol Palaeoecol 252, 586–600.

Clark, P.U., Shakun, J.D., Baker, P.A., Bartlein, P.J., Brewer, S., Brook, E., Carlson, A.E., Cheng, H., Kaufman, D.S., Liu, Z., 2012. Global climate evolution during the last deglaciation. Proceedings of the National Academy of Sciences 109, E1134–E1142

Clegg. M.R., Maberly, S.C., Jones, R.J., 2007. Behavioral response as a predictor of seasonal depth distribution and vertical niche separation in freshwater phytoplanktonic flagellates. Limnol. Oceanogr. 52, 441–455.

Cohen, A.S., 2003. Paleolimnology: The History and Evolution of Lake Systems. Oxford University Press, Oxford

Cohen, J., Barlow, M., 2005. The NAO, the AO, and Global Warming: How Closely Related?. J. Clim. 18(21), 4498-4513.

Comas-Bru, L. and McDermott, F. 2014. Impacts of the EA and SCA patterns on the European twentieth century NAO–winter climate relationship. Q.J.R. Meteorol. Soc., 140: 354–363.

Combourieu Nebout, N., Peyron, O., Dormoy, I., Desprat, S., Beaudouin, C., Kotthoff, U., Marret F., 2009. Rapid climatic variability in the west Mediterranean during the last 25000 years from high resolution pollen data. Clim. Past. 5, 503-521.

Corella, J.P., Brauer, A., Mangili, C., Rull, V., Vegas-Villarrubia, T., Morellon, M., Valero-Garces, B.L., 2012. The 1.5-ka varved record of Lake Montcortes (southern Pyrenees, NE Spain). Quaternary Res. 78, 323-332.

Corella, J.P., Stefanova, V., El Anjoumi, A., Rico, E., Giralt, S., Moreno, A., Plata-Montero, A., Valero-Garcés, B.L., 2013. A 2500-year multi-proxy reconstruction of climate change and human activities in northern Spain: The Lake Arreo record. Palaeogeogr. Palaeocl. 386, 555-568.

Costas, S., Jerez, S., Trigo, R.M., Goble, R., Rebêlo, L., 2012. Sand invasion along the Portuguese coast forced by westerly shifts during cold climate events. Quaternary Sci. Rev. 42, 15–28

Croudace, I.W., Rindby, A. and Rothwell, R.G., 2006: ITRAX: description and evaluation of a new X-ray core scanner. In: Rothwell, R.G., (Ed.) New ways of looking at sediment cores and core data, Geological Society Special Publication, 267: 51-63.

Cowton, T., Hughes, P.D., Gibbard, P.L., 2009. Palaeoglaciation of Parque Natural Lago de Sanabria, northwest Spain. Geomorphology 108, 282–291.

Craig, H., 1957. Isotopic standards for carbon and oxygen and correction factors for mass-spectrometric analysis of carbon dioxide. Geochim. Cosmochim. Ac. 12, 133-149.

de Abreu, L., Shackleton, N.J., Schönfeld, J., Hall, M.A., Chapman, M.R., 2003. Millenial-scale oceanic climate variability off the Western Iberian margin during the last two glacial periods. Mar. Geol. 196(1-2), 1-20.

de Hoyos, C., 1996. Limnología del Lago de Sanabria: variabilidad interanual del fitoplankton. PhD Thesis, Univ. Salamanca, Spain, 438 pp (in Spanish).

de Hoyos, C., Aldasoro, J.J., Toro, M., Comín, F.A., 1998. Specific composition and ecology of chrysophyte flagellates in Lake Sanabria (NW Spain). Hydrobiologia 369/370, 287-295.

de Hoyos, C., Comín, F.A., 1999. The importante of inter-annual variability for management. Hydrobiologia 395/396, 281-291.

Dean, W.E., 1993. Physical properties, mineralogy, and geochemistry of varved sediments from Elk Lake, Minnesota. In: Bradbury, J.P., Dean, W.E., (Eds.). Elk Lake, Minnesota: Evidence for Rapid Climate Change in the North-Central United States, Geological Society of America, Special Paper 276, 135–157pp.

Denys, L., 1991/1992. A check-list of the diatoms in the Holocene deposits of the Western Belgian coastal plain with the survey of their apparent ecological requirements, I. Introduction, ecological code and complete list. Serv. Geol. Belg. Prof. Paper 246.

Desprat, S., Sánchez Goñi, M.F., Loutre, M.F., 2003. Revealing climatic variability of the last three millennia in northwestern Iberia using pollen influx data. Earth Planet. Sc. Lett. 213, 63–78.

Díez-Montes, A., 2006. La geología del Dominio "Ollo de Sapo" en las comarcas de Sanabria y Terra do Bolo. Ph.D. thesis, Universidad de Salamanca, Salamanca, Spain, 512 pp, (in Spanish).

Diz, P., Francés, G., Pelejero, C., Grimalt, J.O., Vilas, F., 2002. The last 3000 years in the Ria de Vigo (NW Iberian Margin): climatic and hydrographic signals. The Holocene 12, 459-468.

Domínguez-Villar, D., Carrasco, R.M., Pedraza, J., Cheng, H., Edwards, R.L., Willenbring, J.K., 2013. Early maximum extent of paleoglaciers from Mediterranean mountains during the last glaciation. Sci. Rep. 3, 2034.

Douglas, M.S.V., Smol, J.P., 1995. Periphytic diatom assemblages from high arctic ponds. J. Phycol. 31, 60–69.

Ehlers, J., Gibbard, P.L., 2007. The extent and chronology of Cenozoic Global Glaciation. Quatern. Int. 164-165, 6-20.

Fletcher, W.J., Sánchez Goñi, M.F., 2008. Orbital- and sub-orbital-scale climate impacts on vegetation of the western Mediterranean basin over the last 48,000 yr. Quaternary Res. 70, 451–464.

García Diez, J.A., 2003: Ribadelago, tragedia de Vega de Tera. Saavedra, (2nd Ed.), Spain.

García-Ruiz, J.M., Martí-Bono, C., Peña-Monné, J.L., Sancho, C., Rhodes, E.J., Valero-Garcés, B., González-Sampériz, P., Moreno, A., 2013. Glacial and fluvial deposits in the Aragón Valley, central-western Pyrenees: chronology of the Pyrenean late Pleistocene glaciers. Geografiska Annaler: Series A, Physical Geography, 95, 15–32.

Genty, D., Blamart, D., Ghaleb, B., Plagnes, V., Causse, C., Bakalowicz, M., Zouari, K., Chkir, N., Hellstrom, J., Wainer, K., Bourges, F., 2006. Timing and dynamics of the last

deglaciation from European and North African $\delta^{13}C$ stalagmite profiles e comparison with Chinese and South Hemisphere stalagmites. Quaternary Sci. Rev. 25, 2118-2142.

Giralt, S., Rico-Herrero, M.T., Vega, J.C., Valero-Garcés, B.L., 2011. Quantitative climate reconstruction linking meteorological, limnological and XRF core scanner datsets: the Lake Sanabria case study, NW Spain. J. Paleolimnol. 46(3), 487-502.

Gladstone, R.M., Ross, I., Valdes, P.J., Abe-Ouchi, A., Braconnot, P., Brewer, S., Kageyama, M., Kitoh, A., LeGrande, A., Marti, O., Ohgaito, R., Otto-Bliesner, B., Peltier, W.R., Vettoretti, G., 2005. Mid-. Holocene NAO: A PMIP2 model intercomparison, Geophys. Res. Lett., 32, L16707, doi:10.1029/2005GL023596.

González-Álvarez, R., Bernárdez, P., Pena, L.D., Francés, G., Prego, R., Diz, P., Vilas, F. 2005. Paleoclimatic evolution of the Galician continental shelf (NW of Spain) during the last 3000 years: from a storm regime to present conditions. J. Marine Syst. 54, 245–60.

González-Villanueva R., Costas S., Pérez-Arlucea M., Jerez S., Trigo R.M., 2013. Effect of climate change in the stabilization and prevailing aeolian activity of a coastal dune (Traba, NW Spain). Geomorphology, 185, 96-119.

González-Sampériz, P., Valero-Garces, B.L., Moreno, A., Jalut, G., Garcia-Ruiz, J.M., Marti-Bono, C., Delgado-Huertas, A., Navas, A., Otto, T., Dedoubat, J.J., 2006. Climate variability in the Spanish Pyrenees during the last 30,000 yr revealed by the El Portalet sequence. Quaternary Res. 66(1), 38-52.

Grootes, P.M., Stuiver, M, White, J.W.C., Johnsen, S., Jouzel, J., 1993. Comparison of Oxygen Isotope Records from the GISP2 and GRIP Greenland Ice Core. Nature, 366, 552-554.

Harris, M.A., Cumming, B.F., Smol, J.P., 2006. Assessment of recent changes in New Brunswick (Canada) Lakes based on paleolimnological shifts in diatom species assemblages. Can. J. Bot. 84, 151-163.

Hansen, H.P., Grasshoff, K., 1983. Automated chemical analysis. In: Grasshoff, K., Ehrhardt, M., Kremling, K. (Eds.), Methods of Seawater Analysis. Verlag Chemie, Weinhein, pp. 368–376.

Heegaard, E., Birks, H.J.B., Telford, R.J., 2005. Relationships between calibrated ages and depth in stratigraphical sequences: an estimation procedure by mixed effect regression. The Holocene 15, 612-618.

Hollander, D.J., Mackenzie, J.A., 1991. CO_2 control on carbon-isotope fractionation during aqueous photosynthesis: a paleo-pCO_2 barometer. Geology 19, 929–932.

Houk, V., 2003. Atlas of freshwater centric diatoms with a brief key and descriptions. Part I., Melosiraceae, Orthoseiraceae, Paraliaceae and Aulacoseiraceae. Czech Phycology. Supplement 1, 1-111.

Houk, V., Klee, R., Tanaka, H., 2010. Atlas of freshwater centric diatoms with a brief key and descriptions, Part III., Stephanodiscaceae A, Cyclotella, Tertiarius, Discostella. Fottea 10 (Supplement), 1–498.

Hurrell, J.W., 1995. Decadal trends in the North Atlantic Oscillation: regional temperatures and precipitation. Science 269, 676-679.

Isarin, R.F.B., Renssen, H., Vandenberghe, J., 1998. The impact of the North Atlantic Ocean on the Younger Dryas climate in northwestern and central Europe. J. Quaternary. Sci. 13(5), 447–453.

Ivy-Ochs, S., Kerschner, H., Maisch, M., Christl, M., Kubik, P.W., Schlüchter, C., 2009. Latest Pleistocene and Holocene glacier variations in the European Alps. Quaternary Sci Rev 28, 2137–2149.

Jalut, G., Turu i Michels, V., Deboubat, J.J., Otto, T., Ezquerra, J., Fontugne, M., Belet, J.M., Bonnet, L., García de Celis, G., Redondo-Vega, J.M., Vidal-Romaní, J.R., Santos, L., 2010. Paleoenvironmental studies in NW Iberia (Cantabrian range): Vegetation history and synthetic approach of the last deglaciation phases in the western Mediterranean. Palaeogeogr. Palaeocl. 297(2), 330-350.

Jerez, S., Trigo, R.M., 2013. Time-scale and extent at which large-scale circulation modes determine the wind and solar potential in the Iberian Peninsula. Environ. Res. Lett. 8 044035 doi:10.1088/1748-9326/8/4/044035

Jiménez-Sánchez, M., Farias Arquer, P., 2002. New radiometric and geomorphologic evidences of a last glacial maximum older than 18 ka in SW European mountains: the example of Redes Natural Park (Cantabrian Mountains, NW Spain). Geodin. Acta 15, 93-101.

Jiménez-Sánchez, M., Rodríguez-Rodríguez, L., García-Ruiz, J.M., Domínguez-Cuesta, M.J., Farias, P., Valero-Garcés, B., Moreno, A., Rico, M., Valcárcel, M., 2012. A review of glacial geomorphology and chronology in northern Spain: Timing and regional variability during the last glacial cycle. Geomorphology 196, 50-64.

Julià, R., Luque, J.A., 2006. Climatic changes vs. catastrophic events in lacustrine systems: A geochemical approach. Quatern. Int. 158, 162-171.

Julià, R., Luque, J.A., Riera, S. Alejandro, J.A., 2007. Climatic and land use changes on the NW of Iberian Peninsula recorded in a 1,500-year record from Lake Sanabria. Contribution to Science 3(3), 355-369.

Karst-Riddoch, T.L., Pisaric, M.F.J., Smol, J.P., 2005. Diatom responses to 20th century climate-related environmental changes in high-elevation mountain lakes of the northern Canadian Cordillera. J. Paleolimnol. 33, 265-282.

Kilman, S., Theriot, E.C., Fritz, S.C., 1996. Linking planktonic diatoms and climate change in the large lakes of the Yellowstone ecosystem using resource theory. Limnol. Oceanogr. 41, 1052-1062.

Lange-Bertalot, H., 2000-2011. Diatoms of the European Inland Waters and Comparable Habitats. Edited by Horst Lange-Bertalot H. Volumes 1-6.

Lebreiro, S., Frances, G., Abrantes, F., Diz, P., Bartels-Jonsdottir, H., Stroynowski, Z.N., Gil, I., Pena, L.D., Rodrigues, T., Jones, P.D., Nombela, M.A., Alejo, I., Briffa, K.R., Harris, I., Grimalt, J.O., 2006. Climate change and coastal hydrographic response along the Atlantic Iberian margin (Tagus Prodelta and Muros Ría) during the last two millennia. The Holocene 16, 1003-1015.

Leira M., 2005. Diatom response to Holocene environmental change in a lake of the northwestern Iberian Peninsula. Quatern. Int. 140-141, 90-102.

Leira, M., Santos, L., 2002. An early Holocene short climatic event in the northwest Iberian Peninsula inferred from pollen and diatoms. Quatern. Int. 93-94, 3-12.

Leroy, S.A.G., Zolitschka, B., Negendank, J.F.W, Seret, G., 2000. Palynological analyses in the laminated sediment of Lake Holzmaar (Eifel, Germany): duration of Lateglacial and Preboreal biozones. Boreas 29, 52-71.

Lorenzo, M.N., Taboada, J.J., Gimeno, L., 2008. Links between circulation weather types and teleconnection patterns and their influence on precipitation patterns in Galicia (NW Spain). Int. J. Climatol 28, 1493-1505.

Lowe, J.J., Rasmussen, S.O., Björck, S., Hoek, W.Z., Steffensen, J.P., Walker, M.J.C., Yu, Z.C., 2008. The INTIMATE group, 2008. Synchronisation of palaeoenvironmental events in the North Atlantic region during the Last Termination: a revised protocol recommended by the INTIMATE group. Quaternary Sci. Rev. 27, 6–17.

Luque, J.A., 2003. El Lago de Sanabria: un sensor de las oscilaciones climáticas del Atlántico Norte durante los últimos 6000 años. PhD Thesis, Univ. Barcelona, Spain, 446 pp, (in Spanish).

Luque, J.A., Julià, J., 2002. Lake sediment response to land-use and climate change during the last 100 years in the oligotrophic Lake Sanabria (northwest of Iberian Peninsula). Sediment. Geol. 148, 343-355.

Magny, M., Leuzinger, U., Bortenschlager, S., Haas, J.N., 2006. Tripartite climate reversal in Central Europe 5600-5300 years ago, Quaternary Res., 65, 3–19.

Magny, M., De Beaulieu, J., Drescher-Schneider, R., Vannière, B., Walter-Simonnet, A., Miras, Y., Millet, L., Bossuet, G., Peyron, O., Brugiapaglia, E., Leroux, A., 2007. Holocene climate changes in the central Mediterranean as recorded by lake-level fluctuations at Lake Accesa (Tuscany , Italy). Quaternary. Sci. Rev. 26, 1736-1758.

Magny, M., Joannin, S., Galop, D., Vannière, B., Haas, J. N., Bassetti, M., Bellintani, P., Scandolari, R., Desmet, M., 2012. Holocene palaeohydrological changes in the northern Mediterranean borderlands as reflected by the lake-level record of Lake Ledro, northeastern Italy. Quaternary Res. 77, 382–396.

Magny, M., Leroux, A., Bichet, V., Gauthier, E., Richard, H., Walter-Simonnet, A.V., 2013a. Climate, vegetation and land use as drivers of Holocene sedimentation: a case study from Lake Saint-Point (Jura Mountains, eastern France). The Holocene 23, 137–147.

Magny, M., Combourieu Nebout, N., de Beaulieu, J.L., Bout-Roumazeilles, V., Colombaroli, D., Desprat, S., Francke, A., Joannin, S., Peyron, O., Revel, M., Sadori, L., Siani, G., Sicre, M.A., Samartin, S., Simonneau, A., Tinner, W., Vannière, B., Wagner, B., Zanchetta, G., Anselmetti, F., Brugiapaglia, E., Chapron, E., Debret, M., Desmet, M., Didier, J., Essallami, L., Galop, D., Gilli, A., Haas, J.N., Kallel, N., Millet, L., Stock, A., Turon, J.L., Wirth, S., 2013b, North–south palaeohydrological contrasts in the central Mediterranean during the Holocene: tentative synthesis and working hypotheses. Clim. Past Discuss. 9, 1901-1967.

Martrat, B., Grimalt, J.O., Shackleton, N.J., de Abreu, L., Hutterli, M.A., Stocker, T.F., 2007. Four Climate Cycles of Recurring Deep and Surface Water Destabilizations on the Iberian Margin. Science 317, 502-507.

Mayewski, P.A., Rohling, E.J., Stager, J.C., Karlèn, W., Maasch, K.A., Meeker, L.D., Meyerson, E.A., Gasse, F., Van Kreveld, S.A., Holmgren, C.A., Lee-Thorp, J.A., Rosqvist, G., Rack, F., Staubwasser, M., Schneider, R., Steig, E.J., 2004. Holocene climate variability. Quaternary Res. 62, 243-255.

Meese, D.A., Gow, A.J., Alley, R.B., Zielinski, G.A., Grootes, P.M., Ram, M., Taylor, K.C., Mayewski, P.A., Bolzan, J.F., 1997. The Greeneland Ice Sheet Project 2 depth-age scale: Methods and results. J. Geophys. Res. 102, 26411–26423.

Menviel, L., Timmermann, A., Friedrich, T., England, M.H., 2014. Hindcasting the continuum of Dansgaard–Oeschger variability: mechanisms, patterns and timing. Clim. Past 10, 63–77

Meyers, P.A., 2003. Applications of organic geochemistry to paleoli-monological reconstructions: a summary of examples from the Laurentian Great Lakes. Org. Geochem. 34(2), 261-289.

Morales-Molino, C., García-Antón, M., 2014. Vegetation and fire history since the last glacial maximum in an inland area of the western Mediterranean Basin (Northern Iberian Plateau, NW Spain) Quaternary Res 81(1), 63–77

Morellón, M., Valero-Garcés, B., Vegas, T., González-Sampériz, P., Delgado-Huertas, A., Mata, P., Moreno, A., Rico, M., Corella, J.P., 2009. Late glacial and Holocene palaeohydrology in the western Mediterranean region: the Lake Estanya record (NE Spain). Quaternary Sci. Rev. 28, 2582–2599.

Morellón, M., Valero-Garcés, B., González-Sampériz, P., Vegas-Vilarrúbia, T., Rubio, E., Rieradevall, M., Delgado-Huertas, A., Mata, P., Romero, O., Engstrom, D.R., López-Vicente, M., Navas, A., Soto, J., 2011. Climate changes and human activities recorded in the sediments of Lake Estanya (NE Spain) during the Medieval Warm Period and Little Ice Age. J. Paleolimnol. 46(3), 423-452.

Morellón, M., Pérez-Sanz, A., Corella, J.P., Büntgen, U., Catalán, J., González-Sampériz, P., González-Trueba, J.J., López-Sáez, J.A., Moreno, A., Pla, S., Saz-Sánchez, M. A., Scussolini, P., Serrano, E., Steinhilber, F., Stefanova, V., Vegas-Vilarrúbia, T., Valero-Garcés, B., 2012. A multi-proxy perspective on millennium-long climate variability in the Southern Pyrenees. Clim. Past Discuss. 8, 683–700.

Moreno, A., Valero-Garcés, B., González-Sampériz, P., Rico. M., 2008. Flood response to rainfall variability during the last 2000 years inferred from the Taravilla Lake record (Central Iberian Range), Spain. J. Paleolimnol. 40(3), 943-961.

Moreno, A., Valero-Garcés, B.L., Jiménez-Sánchez, M., Domínguez, M.J., Mata, P., Navas, A., González-Sampériz, P., Stoll, H., Farias, P., Morellón, M., Corella, P., Rico, M., 2010a. The last deglaciation in the Picos de Europa National Park (Cantabrian Mountains, Northern Spain). J. Quaternary Sci. 25(7), 1076-1091.

Moreno, A., Stoll, H., Jiménez-Sánchez, M., Cacho, I., Valero-Garcés, B., Ito, E., Lawrence, E.R., 2010b. A speleothem record of glacial (25–11.6 kyr BP) rapid climatic changes from northern Iberian Peninsula. J. Quaternary Sci. 71(3-4), 218-231.

Moreno, A., López-Merino, L., Leira, M., Marco Barba, J., González-Sampériz, P., Valero-Garcés, B.L., López-Sáez, J.A., Santos, L., Mata, P., Ito, E., 2011. Revealing Holocene environmental history from the multiproxy record of a mountain lake (Lago Enol, N Iberian Peninsula). J. Paleolimnol. 46(3), 327-349.

Moreno, A.; González-Sampériz, P.; Valero-Garcés, B.L., Fletcher W.J. 2012a. Northern Iberian abrupt climate change dynamics during the last glacial cycle: A view from lacustrine sediments. Quaternary Sci. Rev. 36, 139-153

Moreno, A., Pérez, A., Frigola, J., Nieto-Moreno, V., Rodrigo-Gámiz, M., Martrat, B., González-Sampériz, P., Morellón, M., Martín-Puertas, C., Corella, J.P., Belmonte, Á., Sancho, C., Cacho, I., Herrera, G., Canals, M., Grimalt, J.O., Jiménez-Espejo, F., Martínez-Ruiz, F.,Vegas-Vilarrúbia, T., Valero-Garcés, B.L., 2012b. The Medieval Climate Anomaly in the Iberian Peninsula reconstructed from marine and lake records. Quaternary Sci. Rev. 43, 16-32.

Muñoz Sobrino, C., Ramil-Rego, P., Rodríguez Guitián, M.A., 2001. Vegetation in the mountains of northwest Iberia during the last glacial-interglacial transition.Veg. Hist. Archaeobot. 10, 7-21.

Muñoz Sobrino, C., Ramil-Rego, P., Gómez-Orellana, L., 2004. Vegetation of the Lago de Sanabria área (NW Iberia) since the end of the Pleistocene: a palaecological reconstruction on the basis of two new pollen sequences. Veg. Hist. Archaeobot. 13, 1-22.

Muñoz Sobrino, C., Ramil-Rego, P., Gómez-Orellana, L., Díaz Varela, R.A., 2005. Palynological data on major Holocene climatic events in NW Iberia. Boreas 34, 381-400.

Muñoz Sobrino, C., Ramil-Rego, P., Gómez-Orellana, L., 2007. Late Würm and early Holocene in the mountains of northwest Iberia: biostratigraphy, chronology and tree colonization. Veg. Hist. Archaeobot. 16, 223-240.

Muñoz Sobrino, C., Ramil-Rego, P., Gómez-Orellana, L., Ferreiro da Costa, J., Díaz Varela, R.A., 2009. Climatic and human effects on the post-glacial dynamics of Fagus sylvatica L. in NW Iberia. Plant Ecol. 203, 317-340.

Muñoz Sobrino, C., García-Gil, S., Iglesias, J., Martínez Carreño, N., Ferreiro da Costa, J., Díaz Varela, R.A., Judd, A., 2012: Environmental change in the Ría de Vigo, NW

Iberia, since the mid-Holocene: new palaeoecological and seismic evidence. Boreas 41, 578–601.

Muñoz Sobrino, C., Heiri, O, Hazekamp, M., van der Velden, D., Kirilova, E.P., García-Moreiras, I., Lotter, A.F., 2013. New data on the Lateglacial period of SW Europe: a high resolution multiproxy record from Laguna de la Roya (NW Iberia). Quaternary Sci. Rev. 80, 58-77.

Naeher, S., Gilli, A., North, R.P., Hamann, Y., Schubert, C.J., 2013. Tracing bottom water oxygenation with sedimentary Mn / Fe ratios in Lake Zurich, Switzerland, Chem. Geol., 352, 125–133.

Naughton, F., Sanchez Goñi, M.F., Desprat, S., Turon, J.L., Duprat, J., Malaizé, B., Joli, C., Cortijo, E., Drago, T., Freitas, M.C., 2007. Present-day and past (last 25000 years) marine pollen signal off western Iberia. Mar. Micropaleontol. 62, 91–114.

Negro, A .I., de Hoyos, C., Vega, J.C., 2000. Phytoplancton structure and dynamics in Lake Sanabria and Valparaiso reservoir (NW Spain). Hydrobiologia 424, 25-37.

Nesje, A., Matthews, J.A., Dahl, S.O., Berrisford, M.S., Andersson, C., 2001. Holocene glacier fluctuations of Flatebreen and winter precipitation changes in the Jostedalsbreen region, western Norway, based on glaciolacustrine records. The Holocene 11, 267–280.

Ortiz, J.E., Gallego, J.L.R., Torres, T., Díaz-Bautista, A., Sierra, C., 2010. Palaeoenvironmental reconstruction of Northern Spain during the last 8000 cal yr BP based on the biomarker content of the Roñanzas peat bog (Asturias). Org. Geochem. 41, 454–466.

Pena, L.D., Francés, G., Diz, P., Esparza, M., Grimalt, J.O., Nombela, M.A., Alejo, I., 2010. Climate fluctuations during the Holocene in NW Iberia: High and low latitude linkages. Cont. Shelf Res. 30(13), 1487–1496.

Peñalba, C., Arnold, M., Guiot, J., Duplessy, J. C., and Beaulieu, J.L., 1997. Termination of the last glaciation in the Iberian peninsula inferred from the pollen sequence of Quintanar de la Sierra. Quaternary Res. 48, 205-214.

Pérez-Sanz, A. González-Sampériz, P., Moreno, A., Valero-Garcés, B., Gil-Romera, G., Rieradevall, M., Tarrats, P., Lasheras-Álvarez, L., Morellón, M., Belmonte, A., Sancho, C., Sevilla-Callejo, M., Navas, A., 2013. Holocene climate variability, vegetation dynamics and fire regime in the central Pyrenees: the Basa de la Mora sequence (NE Spain). Quaternary Sci. Rev. 73, 149-169.

Ramil-Rego, P., Muñoz Sobrino, C., Rodríguez Guitián, M.A., Gómez-Orellana, L., 1998. Differences in the vegetation of the North Iberian peninsula during the last 16,000 years. Plant Ecol. 138, 41-62.

Rasmussen, S.O., Andersen, K.K., Svensson, A.M., Steffensen, J.P., Vinther, B.M., Clausen, H.B., Siggaard-Andersen, M.L., Johnsen, S.J., Larsen, L.B., Dahl-Jensen D., Bigler M., Röthlisberger, R., Fischer, H., Goto-Azuma, K., Hansson, M.E., Ruth, U., 2006. A new Greenland ice core chronology for the last glacial termination. J. Geophys. Res., 111, D06102, doi:10.1029/2005JD006079

Reimer, P.J., Bard, E., Bayliss, A., Beck, J.W., Blackwell, P.G., Bronk Ramsey, C., Buck, C.E., Edwards, R.L., Friedrich, M., Grootes, P.M., Guilderson, T.P., Haflidason, H., Hajdas, I., Hatté, C., Heaton, T.J., Hoffmann, D.L., Hogg, A.G., Hughen, K.A., Kaiser, K.F., Kromer, B., Manning, S.W., Niu, M., Reimer, R.W., Richards, D.A., Scott, E.M., Southon, J.R., Turney, C.S.M., van der Plicht, J., 2013. IntCal13 and Marine13 radiocarbon age calibration curves, 0-50,000 years cal BP. Radiocarbon 55: 1869-1887

Reavie, E.D., Smol, J.P., 1997. Diatom-based model to infer past littoral habitat characteristics in the St. Lawrence River. J. Great Lakes Res. 23, 339–348.

Reynolds, C.S., 1984. The ecology of freshwater phytoplankton. Cambridge Univ. Pres.

Reynolds, C.S., 2006. Ecology of phytoplankton. Cambridge Univ. Press.

Rivas-Martinez, S., Penas, A., Luengo, M.A., Rivas-Saenz, S., 2003. Worlwide bioclimatic classification system. In: Lieth, H. (Ed.). Cimate and Biosphere, CD series. www.globalbioclimatics.org

Rodrigues, T., Grimalt, J.O., Abrantes, F.G., Flores, J.A., Lebreiro, S.M., 2009. Holocene interdependence of changes in sea surface temperature, productivity, and fluvial inputs in the Iberian continental shelf (Tagus mud patch). Geochem. Geophys. Geosyst. 10, Q07U06.

Rodrigues, T., Grimalt, J.O., Abrantes, F., Naughtona F., Flores J.A., 2010. The last glacial–interglacial transition (LGIT) in the western mid-latitudes of the North Atlantic: Abrupt sea surface temperature change and sea level implications. Quaternary Sci. Rev 29(15–16), 1853–1862.

Rodríguez-Rodríguez, L., Jiménez-Sánchez, M., Domínguez-Cuesta, M.J., Rico, M.T., Valero-Garcés, B., 2011. Last deglaciation in northwestern Spain: New chronological and geomorphologic evidence from the Sanabria region. Geomorphology. 135(1–2), 48–65.

Rodríguez-Rodríguez, L., Jiménez-Sánchez, M., Domínguez-Cuesta, M.J., Rinterknech, V., Pallàs, R., Bourlès, D., Valero-Garcés, B., 2014. A multiple dating-method approach applied to the Sanabria Lake moraine complex (NW Iberian Peninsula, SW Europe). Quaternary Sci. Rev. 83, 1-10.

Rodrigo-Gámiz, M., Martínez Ruiz, F., Jiménez Espejo, F.J., Gallego Torres, D., Nieto Moreno, V., Martín Ramos, D., Ariztegui, D., Romero, O., 2011. Impact of climate variability in the western Mediterranean during the last 20,000 years: oceanic and atmospheric responses. Quaternary Sci. Rev. 30(15-16), 2018- 2034.

Round, F.E., Crawford, R.M., Mann, D.G., 1990. The Diatoms, Biology & Morphology of the Genera. Cambridge University Press, Cambridge.

Rühland, K., Smol, J.P., 2005. Diatom shifts as evidence for recent subarctic warming in a remote tundra lake, NWT, Canada. Palaeogeogr. Palaeoclim. Palaeocl. 226, 1–16.

Ruiz de la Torre, J. (1996) Mapa forestal de España (1:200.000) (MFE200) Ponferrada. 3-3. Ministerio de Agricultura, Pesca y Alimentación. ICONA. Spain.

Sabater, S., Haworth, E.Y., 1995. An assessment of recent trophic changes in Windermere South Basin (England) based on diatom remains and fossil pigments. J. Paleolimnol. 14, 151-163.

Saz Sánchez, M.A., 2003, Temperaturas y precipitaciones en la mitad norte de España desde el siglo XV. Estudio dendroclimático. Consejo de Protección de la Naturaleza. Diputación General de Aragón. Spain.

Santos, L., Vidal-Romaní, J.R., Jalut, G., 2000. History of vegetation during the Holocene in the Courel and Queixa Sierras, Galicia, northwest Iberian Peninsula. J. Quaternary Sci. 15(6), 621–632.

Schellekens, J., Buurman, P., Fraga, I., Martínez-Cortizas, A., 2011. Holocene vegetation and hydrologic changes inferred from molecular vegetation markers in peat, Penido Vello (Galicia, Spain). Palaeogeogr Palaeoclimatol Palaeoecol 299, 56–69

Schnurrenberger, D.W., Russell, J.M., Kelts, K.R., 2003. Classification of lacustrine sediments based on sedimentary components. J. Paleolimnol. 29(2), 141-154.

Simonneau, A., Chapron, E., Courp, T., Tachikawa, K., Roux, G.,Baron, S., Galop, D., Garcia. M., Di Giovanni, C.1, Motelica-Heino, M., Mazier, F., Foucher, A., Houet, T., Desmet, M., Bard, E., 2013a. Recent climatic and anthropogenic imprints on lacustrine

systems in the Pyrenean Mountains inferred from minerogenic and organic clastic supply (Vicdessos valley, Pyrenees, France). The Holocene 23 (12), 1764-1777

Simonneau, A., Chapron, E., Vannière, B., Wirth, S. B., Gilli, A., Di Giovanni, C., Anselmetti, F. S., Desmet, M., Magny, M., 2013b. Mass-movement and flood-induced deposits in Lake Ledro, southern Alps, Italy: implications for Holocene palaeohydrology and natural hazards. Clim. Past, 9, 825–840.

Sofer, Z., 1980. Preparation of carbon dioxide for stable carbon isotope analysis of petroleum fractions. Anal. Chem. 52, 1389-1391

Spötl, C., Nicolussi, K., Patzelt, G., Boch, R., 2010. Humid climate during deposition of sapropel 1 in the Mediterranean Sea: Assessing the influence on the Alps. Global Planet Change 71, 242–248.

Stoll, H.M., Moreno, A., Mendez-Vicente, A., Gonzalez-Lemos, S., Jimenez-Sanchez, M., Dominguez-Cuesta, M.J., Edwards, R.L., Cheng, H., Wang, X., 2013. Paleoclimate and growth rates of speleothems in the northwestern Iberian Peninsula over the last two glacial cycles. Quaternary Res. 80(2), 284-290.

Street, J.H., Anderson, R.S., Paytan A., 2102. An organic geochemical record of Sierra Nevada climate since the LGM from Swamp Lake, Yosemite. Quaternary Sci. Rev. 40, 89-106.

Stuiver, M., Reimer, P. J., Reimer, R. W. 2005. CALIB 5.0. [program and documentation]. http://calib.qub.ac.uk/calib/

Trigo, R.M, Osborn, T.J., Corte-Real, J.M., 2002 The North Atlantic Oscillation influence on Europe: climate impacts and associated physical mechanisms. Clim. Res. 20, 9–17, 2002

Trigo, R.M., Pozo-Vázquez, D., Osborne, T., Castro-Díez, Y., Gómiz-Fortis, S., Esteban-Parra, M.J., 2004. North Atlantic Oscillation influence on precipitation, river flow and water resources in the Iberian peninsula. Int. J. Climatol. 24, 925–944.

Trigo, R.M., Valente, M.A., Trigo, I.F., Miranda, P.M.A., Ramos, A.M., Paredes, D., García-Herrera, R., 2008. The Impact of North Atlantic Wind and Cyclone Trends on European Precipitation and Significant Wave Height in the Atlantic. Annals of the New York Academy of Sciences, 1146(1), 212-234.

Trouet, V., Esper, J., Graham, N.E., Baker, A., Scourse, J.D., Frank, D.C., 2009. Persistent Positive North Atlantic Oscillation Mode Dominated the Medieval Climate Anomaly. Science 324, 78-80.

van der Knaap, W.O., van Leeuwen, J.F.N., 1997. Late Glacial and Early Holocene vegetation succession altitudinal vegetation zonation, and climatic change in the Serra da Estrela, Portugal. Rev. Palaeobot. Palynol. 97, 239- 285.

Vannière, B., Magny, M., Joannin, ,S., Simonneau, A., Wirth, S.B., Hamann, Y.,Chapron, E., Gilli4, A., Desmet, M., Anselmetti, F.S. 2013. Orbital changes, variation in solar activity and increased anthropogenic activities: controls on the Holocene flood frequency in the Lake Ledro area, Northern Italy. Clim. Past, 9, 1193–1209.

Vega, J.C., de Hoyos, C., Aldasororo, J.J., 1992. The Sanabria Lake: the largest natural freshwater lake in Spain. Limnetica 8, 49-57.

Vega, J.C., de Hoyos, C., Aldasoro, J.J., de Miguel, J., Fraile, H., 2005. Nuevos datos morfométricos para el Lago de Sanabria. Limnetica 24(1-2), 115-122.

Vicente-Serrano, S.M., López-Moreno, J.I., 2008. Nonstationary influence of the North Atlantic Oscillation on European precipitation. J. Geophys. Res. 113, D20120

Vinther, B.M., Andersen, K.K., Jones, P.D., Briffa, K.R., Cappelen, J., 2006. Extending Greenland temperature records into the late eighteenth century. J. Geophys. Res.,111, D11105, doi:10.1029/2005JD006810

Wanner H., Beer J., Bütikofer J., Crowley T.J., Cubasch U., Flückiger J., Goosse H., Grosjean M., Joos F., Kaplan J.O., Küttel M., Müller S.A., Prentice I.C., Solomina O., Stocker T.F., Tarasov P., Wagner M. and Widmann M. 2008. Mid- to Late Holocene climate change: an overview. Quaternary Sci. Rev. 27, 1791-1828.

Wetzel, R.G., 1983. Limnology. Saunders College Publishing, Philadelphia.

Wolin, J.A., Stoermer, E.F., 2005. Response of a Lake Michigan coastal lake to anthropogenic catchment disturbance. J. Paleolimnol. 33, 73–94.

Zhao, C., Yu, Z., and Zhao, Y. 2010. Holocene climate trend, variability, and shift documented by lacustrine stable-isotope record in the northeastern United States, Quaternary Sci. Rev., 29, 1831–1843.

Figure captions

Fig. 1 A. Location of Sanabria Lake (red star), marine and continental records on the biogeographic map of Europe (modified from www.globalbioclimatics.org), 1: GISP2 ice core (Grootes et al., 1993; Meese et al., 1997); 2: VM29-191 (Bond et al., 1997); 3) MD03-2697 (Naughton et al., 2007); 4: MD99-2331 (Naughton et al., 2007); 5: CGPL00-1 (González Álvarez et al., 2005); 6: MD9045 (de Abreu et al., 2003); 7: MD03-2699 (Rodrigues et al., 2010); 8: D13902 and P0287 (Abrantes et al., 2005,

2011); 9: Lake Saint-Point (Magny et al., 2013a); 10: Lake Ledro (Magny et al., 2013b; Vannière et al., 2013; Simonneau et al., 2013a); 11: Lake Accesa (Magny et al., 2013 b). The rectangle indicates Fig. 1B location. B Map of northern Iberia showing the study site (red star) and the main paleoecological and paleoclimatic records discussed in the text. Purple circles correpond to lacustrine records, gray circles to peat bog records, black triangle to speleothems records, and blue square to shallow marine records. Continental sequences 1: Lake Sanabria (Luque and Juliá, 2002; Luque, 2003; Julià and Luque 2006; Julià et al., 2007; Giralt et al., 2011); 2: Lleguna (Muñoz Sobrino et al., 2004) preiviously named Sanabria Marsh (Allen et al., 1996) 3: Laguna de Sanguijuelas (Muñoz-Sobrino et al., 2004); 4: Ayoó mire (Morales-Molino and García-Antón, 2014); 5: Laguna Roya (Allen et al., 1996; Muñoz Sobrino et al., 2013); 6: Lagoa de Marinho (Ramil-Rego et al, 1998); 7: Laguna Lucenza (Santos, 2000; Muñoz Sobrino et al., 2001; Leira and Santos, 2002); 8: Lagoa Grande (Leira, 2005); 9: Penido Vello peat bog (Schellekens et al., 2011); 10: Chan do Lamoso (Ramil-Rego et al, 1998); 11: La Mata (Jalut et al., 2010); 12: Lago Enol (Moreno et al., 2011); 13: Roñanzas peat bog (Ortiz et al., 2010); 14: Pindal cave (Moreno et al., 2010a; Stoll et al., 2013); 15: Puerto de los Tornos peatbog (Muñoz-Sobrino et al., 2009); 16: Lake Arreo (Corella et al., 2013); 17: Quintanar de la Sierra (Peñalba et al., 1997); 18: Portalet (González-Samperiz et al., 2006); 19: Basa de la Mora (Pérez-Sanz et al., 2013); 20: Estanya Lake (Morellón et al., 2009; 2011); 21: Montcortés (Corella et al., 2012); 22: Lake Majeur-French Pyrenees (Simonneau et al., 2013a); 23: Taravilla Lake (Moreno et al., 2008) 24: Eagle cave (Domínguez-Villar et al., 2013); 25: Charco da Candieira (van der Knaap and van Leeuwen, 1997). The marine cores represented on the map are 26: SMP02-3 (Bernárdez et al., 2008); 27: VIR-18 (Diz et al., 2002; Desprat et al., 2003) and VIR-94 (Muñoz Sobrino et al., 2012); 28: EUGC-3B (Lebreiro et al., 2006; Pena et al., 2010). The square indicates Figs. 1C-H location. C: Sanabria Lake basin showing the location of the nearby records (modified from http://atlas.itacyl.es), D: Map of elevation (modified from www.idecyl.jcyl.es); E: Geological map (based on Díaz-Montes, 2006); F: Soil map (http://atlas.itacyl.es); G). Vegetation Biomes in Sanabria drainage basin (based in Ruiz de la Torre, J. 1996); H: Map of land use (www.ign.es).

Fig. 2. Bathymetric map of Sanabria Lake (modified from Vega et al., 2005), N-S and E-W depth sections and location of the Kullenberg cores in both sub-basins.

Fig. 3. Sanabria cores correlation using sedimentary facies and magnetic susceptibility values: A) Cores 1A and 4A in the western sub-basin. B) Cores 2A and 3A in the eastern sub-basin. C) Short core 2007-1M from the eastern sub-basin.

Fig. 4. A) Depth- Age model and sedimentation rates for Sanabria SAN04-3A core. Chronological model based on a mixed effect regression function (Heegaard et al., 2005). B) Age model for SAN07-2M determined by ^{14}C (blue) and ^{210}Pb (green) (constant rate of supply model) dates. C) Total ^{210}Pb activity obtained by gamma spectrometry in core 2M.

Fig. 5. Core SAN04-3A: AMS ^{14}C ages, core image, sedimentary facies and units, magnetic susceptibility, Lightness, TOC, TN, C/N, biogenic silica, and main depositional environments.

Fig. 6. Selected elements and geochemical ratios for SAN04-3A core.

Fig. 7. The last 500 years in SAN07-1M and SAN07-2M cores: core image, MS (from core 1M) and sedimentary facies and units, TOC, TN, C/N, $\delta^{13}Corg$, biogenic silica and main diatom taxa. The grey stripes indicate less organic-rich intervals (1959 AD and 1570-1760 AD)

Fig. 8. Main diatom taxa from SAN04-3A and SAN07-2M cores

Fig. 9. Comparison of the last 14 kyrs in the Sanabria sequence with other records. The grey bands indicate lower humidity periods. (a) Compilation of data from core SAN04-3A; (b) hematite stained grains percentage (%HSG) at core VM 29-191 (Bond et al., 1997); (c) Continuous and 290-year running mean records of the oxygen isotopic profile from the GISP2 ice core (Grootes et al., 1993; Meese et al., 1997); (d) Holocene rapid climate changes from Mayewski et al. (2004), green stripes indicate rapid climate change (RCC) events; (e) Benthic foraminifera (Nonion commune) $\delta^{13}C$ record from core EUGC-3B (NW Iberia) (Pena et al., 2010); yellow stripes indicate positive $\delta^{13}C$ excursions (less rainfall due to a southward shift in the main position of the storm tracks); (f) Lake level record of Accesa and Ledro lakes

(Italy) (Magny et al., 2007, 2012); (g) Planktonic foraminifera (G. Bulloides) $\delta^{18}O$ from core MD95-2040 (W Iberia) (de Abreu et al., 2003); (h) Summarised pollen diagram from Sanabria Marsh (Allen et al., 1996) which correspond to Lleguna site (Muñoz Sobrino et al., 2004).

Table 1.- Radiocarbon (^{14}C AMS) dates obtained from Sanabria Lake cores SAN04-3A-1K and SAN07-2M. Calibration based on Reimer et al. (2013). The date in italics (*Poz-23636*) has been excluded of the age model (see text).

Core	Core Depth (cm)	Laboratory code	Type of samples	^{14}C-age BP	Calibrated Age (cal BP) (range 2σ)	Calendar Age (cal AD/BC)
SAN04-3A-1K	14	Poz-23630	plant remains	1020 ± 40	950 ± 51	1000 ± 51 AD
	54	Poz-20090	plant remains	1330 ± 30	1266 ± 35	684 ± 35 AD
	127	Poz-23631	plant remains	2130 ± 100	2118 ± 221	168 ± 221 BC
	254	Poz-20091	bulk sediment	2985 ± 35	3155 ± 98	1205 ± 98 BC
	310	Poz-23634	plant remains	2935 ± 30	3076 ± 97	1126 ± 97 BC
	353	Poz-20092	bulk sediment	3645 ± 35	3942 ± 72	1992 ± 72 BC
	474	Poz-23635	plant remains	5070 ± 40	5820 ± 92	3870 ± 92 BC
	474	Poz-23673	bulk sediment	5250 ± 40	6022 ± 99	4072 ± 99 BC
	538	Poz-20093	bulk sediment	6710 ± 40	7582 ± 75	5632 ± 75 BC
	668	Poz-20094	bulk sediment	9530 ± 50	10887 ± 204	8937 ± 204 BC
	707	Poz-23674	bulk sediment	10340 ± 50	12194 ± 203	10244 ± 203 BC
	717	Poz-23675	bulk sediment	11240 ± 50	13116 ± 96	11166 ± 96BC
	728	Poz-20095	plant remains	12330 ± 60	14390 ± 311	12440 ± 311 BC
	873	*Poz-23636*	*plant remains*	*5140 ± 35*	*5862 ± 69*	*3912 ± 69 BC*
	891	Poz-12367	bulk sediment	21460 ± 140	25760 ± 260	23810 ± 260 BC
SAN07-2M	36.5	Poz-22399	plant remains	140 ± 30	225 ± 56	1730 ± 56 AD

Table 2. Main sedimentary facies in Sanabria Lake sequence.

Facies Association	Facies	Sedimentological Features	Composition	Depositional Environment (and Processes)
Clastic. Sediments are mostly composed by quartz, micas, feldspars and clay minerals. Very low organic matter content and high detrital-related elements (K, Ti).	**A**	Dm – thick massive to slightly banded light greenish gray fine to medium silt.	**TOC**=0.1-0.3% **TN**=0.03-0.06% **C/N**=3.2-10.8 **$\delta^{13}C_{org=}$**-22.4/-25.6‰ **BioSi**=0.9-1.5% **MS**=15-27x10^{-5} SI **L***=51-66	Proglacial lake (meltwater fluxes)
	B	Cm to dm – thick massive sand in lenses and irregular pockets some with iron oxides.	**TOC**=0.2-0.3% **TN**=0.03-0.04% **C/N**=6.2-14.2 **$\delta^{13}C_{org=}$**-20.6/-14.7‰ **BioSi**=0.9-1.2% **MS**=23-28x10^{-5} SI **L***=56-85	Proglacial lake (strong meltwater fluxes)
Clastic - organic	**C**	Cm- thick, laminated, dark gray silt with variable organic matter content and higher detrital-related elements (K, Ti).	**TOC**=0.7-3.8% **TN**=0.08-0.4% **C/N**=11.4-13.0 **$\delta^{13}C_{org=}$**-24.8/-26.5‰ **BioSi**=1.2-3% **MS**=8-12x10^{-5} SI **L***=22-41	Glacio-lacustrine (strong glacier influence)
	D	Cm to dm thick, faintly laminated, very dark grayish brown organic-rich silts with abundant plant remains. Lower detrital-related elements (K, Ti) and higher As values.	**TOC**=4.1-5.3% **TN**=0.5-0.6% **C/N**=8.3-11.4 **$\delta^{13}C_{org=}$**-26.8/-27.1‰ **BioSi**=8.4-9.8% **MS**=4-7x10^{-5} SI **L***=11-18	Glacio-lacustrine (lake processes dominate)
	E	Cm- thick fining upward layers composed of grey fine sand (low organic matter content and higher detrital-related elements (K, Ti) and fine, more organic silts.	**TOC**=3.0-7.3% **TN**=0.3-0.6% **C/N**=13.0-13.9 **$\delta^{13}C_{org=}$**-26.5/-26.1‰ **BioSi**=2.7-7.5% **MS**=9-12x10^{-5} SI **L***=12-60	Glacio-lacustrine (meltwater fluxes and lacustrine)
Organic	**F**	Dm- to up to 1 m thick layers of massive, dark greyish brown to dark olive brown organic ooze to fine organic-rich silt, with low detrital-related elements (K, Ti)	**TOC**=10.5-12.8% **TN**=0.8-1.0% **C/N**=14.2-15.3 **$\delta^{13}C_{org=}$**-27.1/-26.7‰ **BioSi**=6-7% **MS**=4-6x10^{-5} SI **L***=3-5 **mean grain size**=15-23µm	Distal, lacustrine (low fluvial input, organic deposition)
	G	Cm-thick layers of laminated to banded light brown to grey silts with some plant remains, with variable organic and inorganic content.	**TOC**=7.7-11.1% **TN**=0.6-0.8% **C/N**=12.5-14.5 **$\delta^{13}C_{org=}$**-27.8/-26.4‰ **BioSi**=5-6% **MS**=5-10x10^{-5} SI **L***=5-7 **mean grain size**=24-27µm	Distal, lacustrine (High fluvial input)
	Ha	Fining upward layers with sandy basal sublayer and massive to subtly laminated light grey silt. High detrital-related elements (K, Ti).	**TOC**=2.6-7.2% **TN**=0.3-0.6% **C/N**=12-15 **$\delta^{13}C_{org=}$**-26.7/-26.2‰ **BioSi**=4-5% **MS**=7-10x10^{-5} SI **L***=10-57 **mean grain size**=25-35µm	Distal lacustrine (Turbidite)
	Hb	Coarsening-fining upward layer composed of grey silts with low organic matter and high detrital related elements (K, Ti).	**TOC**=2-6% **TN**=0.3-0.5% **C/N**=14-16 **$\delta^{13}C_{org=}$**-26.2/-25.7‰ **BioSi**=2-3% **MS**=30-37x10^{-5} SI **L***=11-22 **mean grain size**=35-58µm	Distal (‘antrophogenic flashflood’ 1959 AD-Dam failure)

Fig. 1

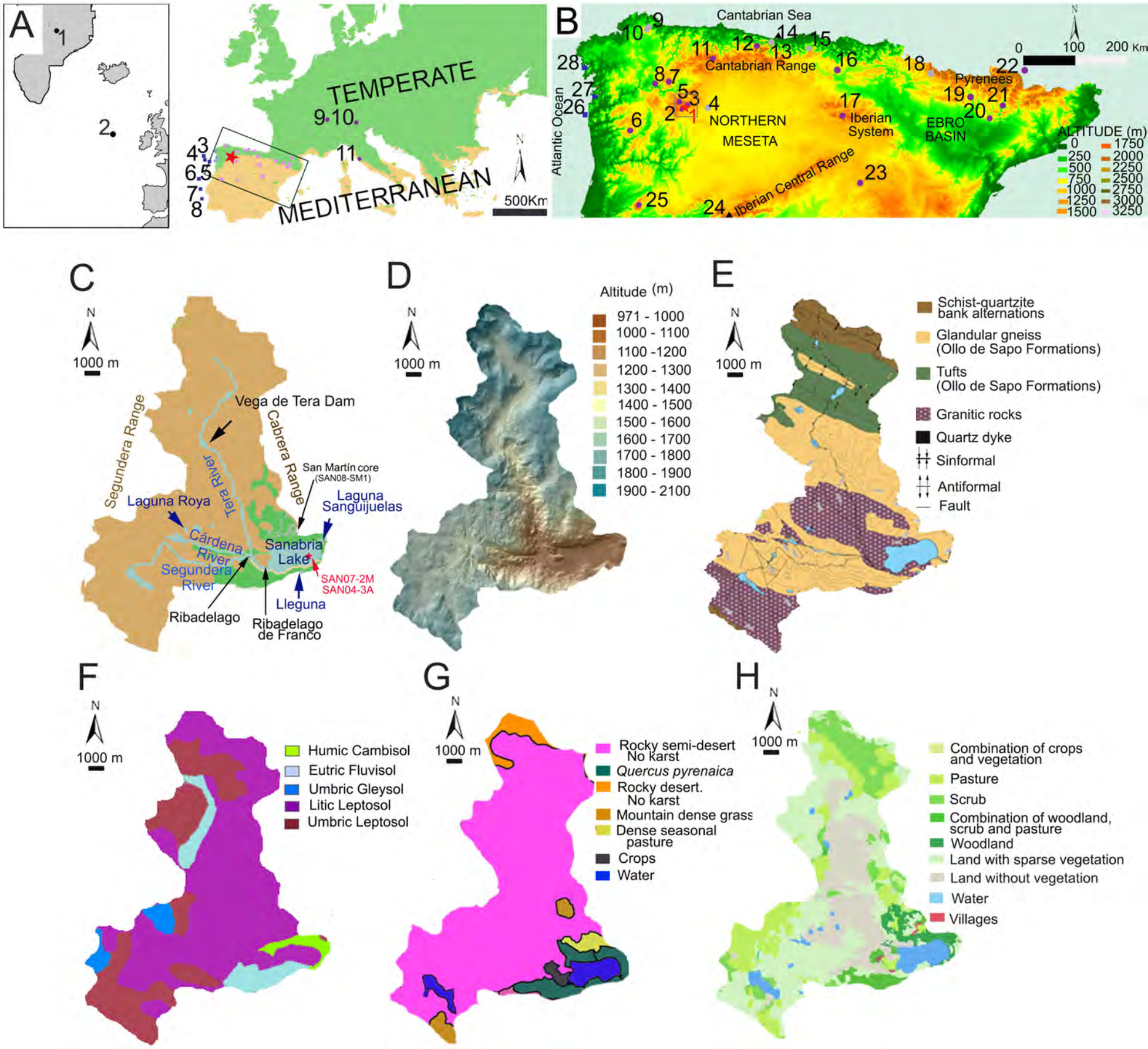
A
1
2
TEMPERATE
MEDITERRANEAN
500Km
B
Cantabrian Sea
Cantabrian Range
Atlantic Ocean
NORTHERN
MESETA
Iberian
System
EBRO
BASIN
Pyrenees
Iberian Central Range
0
100
200 Km
ALTITUDE (m)
0
250
500
750
1000
1250
1500
1750
2000
2250
2500
2750
3000
3250
C
1000 m
Vega de Tera Dam
Segundera Range
Tera River
Cabrera Range
San Martín core
(SAN08-SM1)
Laguna Roya
Laguna
Sanguijuelas
Cárdena
River
Segundera
River
Sanabria
Lake
SAN07-2M
SAN04-3A
Lleguna
Ribadelago
Ribadelago
de Franco
D
1000 m
Altitude (m)
971 - 1000
1000 - 1100
1100 -1200
1200 - 1300
1300 - 1400
1400 - 1500
1500 - 1600
1600 - 1700
1700 - 1800
1800 - 1900
1900 - 2100
E
1000 m
Schist-quartzite
bank alternations
Glandular gneiss
(Ollo de Sapo Formations)
Tufts
(Ollo de Sapo Formations)
Granitic rocks
Quartz dyke
Sinformal
Antiformal
Fault
F
1000 m
Humic Cambisol
Eutric Fluvisol
Umbric Gleysol
Litic Leptosol
Umbric Leptosol
G
1000 m
Rocky semi-desert
No karst
Quercus pyrenaica
Rocky desert.
No karst
Mountain dense grass
Dense seasonal
pasture
Crops
Water
H
1000 m
Combination of crops
and vegetation
Pasture
Scrub
Combination of woodland,
scrub and pasture
Woodland
Land with sparse vegetation
Land without vegetation
Water
Villages

Fig. 2

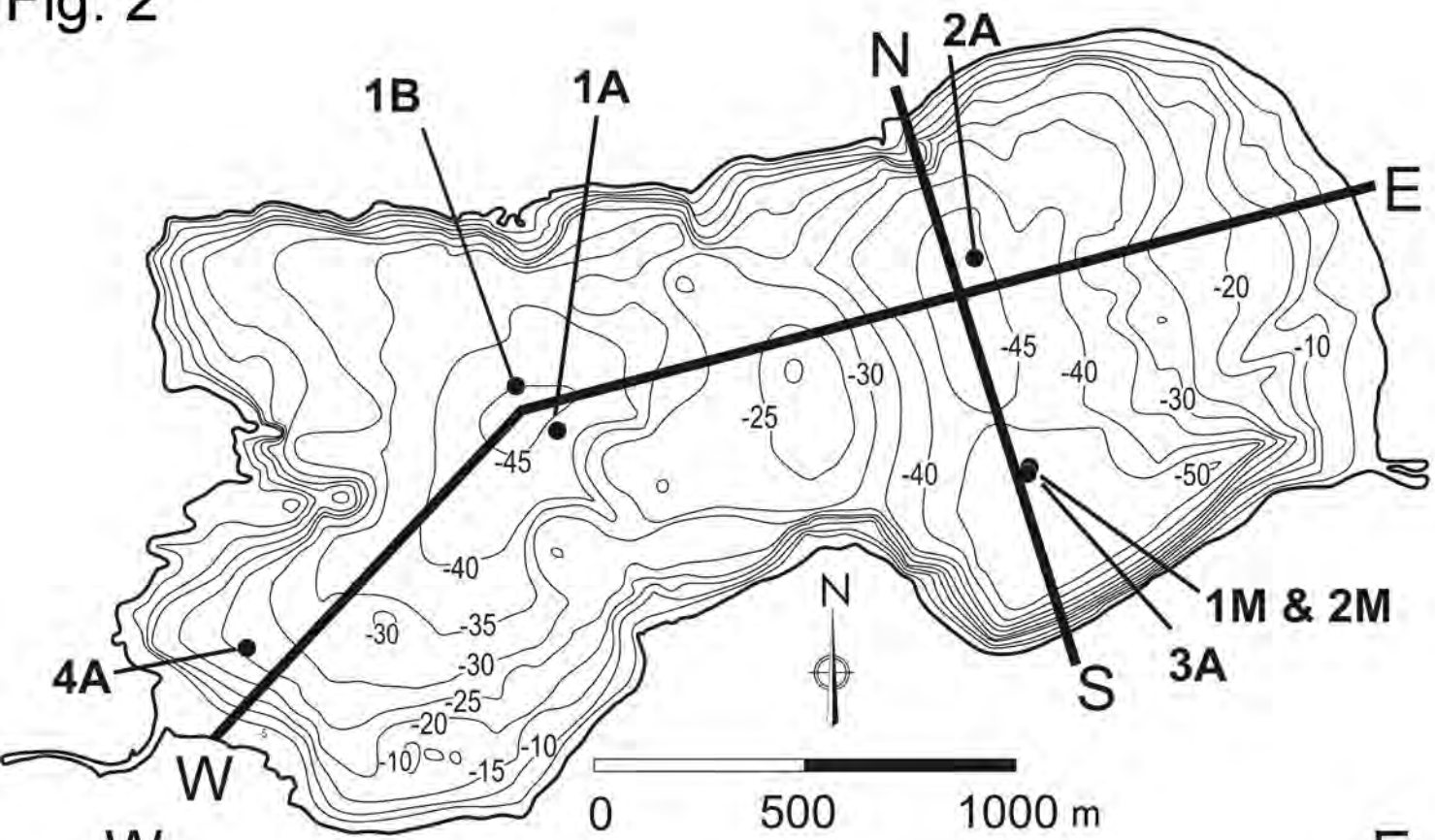
1B
1A
N
2A
E
-20
-10
-45
-40
-30
-25
-30
-45
-40
-50
-40
-30
-35
-30
-25
-20
-10
-15
-10
4A
W
N
1M & 2M
3A
S
0
500
1000 m

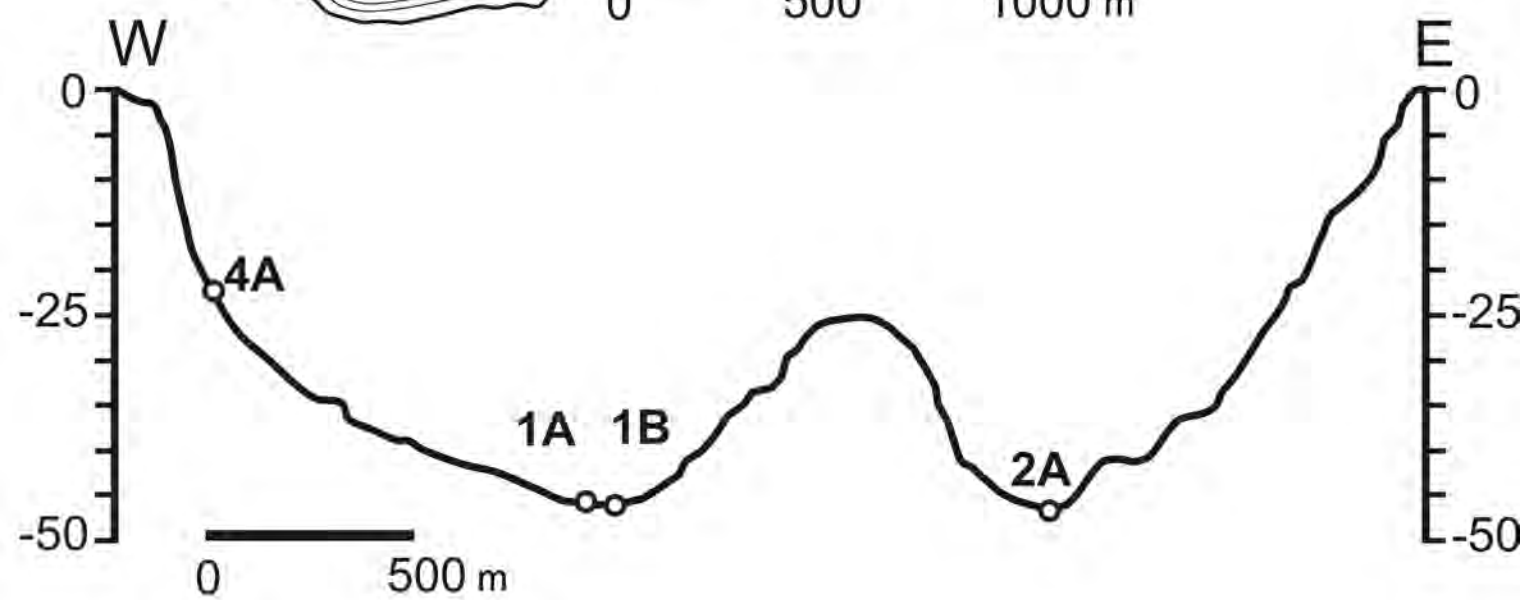
W
E
0
-25
-50
4A
1A 1B
2A
0
500 m

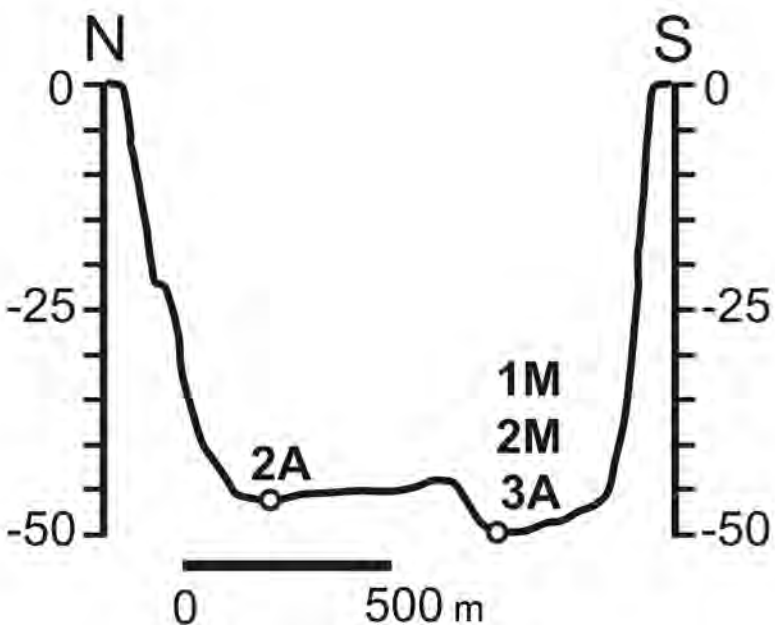
N
S
0
-25
-50
2A
1M
2M
3A
0
500 m

Fig. 3.

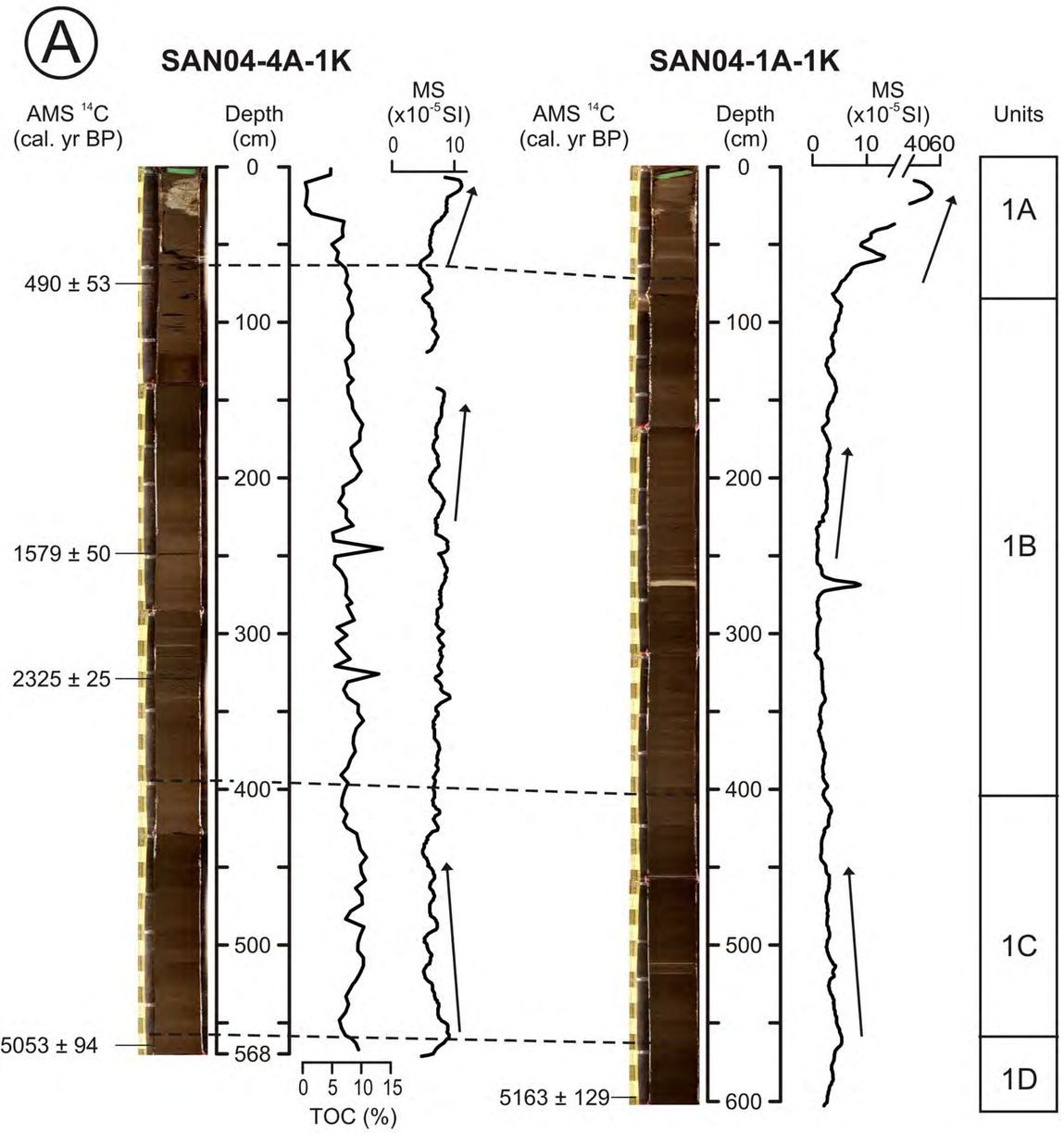
A
SAN04-4A-1K
AMS 14C (cal. yr BP)
Depth (cm)
MS (x10-5SI)
0 10
490 ± 53
1579 ± 50
2325 ± 25
5053 ± 94
0
100
200
300
400
500
568
0 5 10 15
TOC (%)
SAN04-1A-1K
AMS 14C (cal. yr BP)
Depth (cm)
MS (x10-5SI)
0 10 40 60
5163 ± 129
0
100
200
300
400
500
600
Units
1A
1B
1C
1D

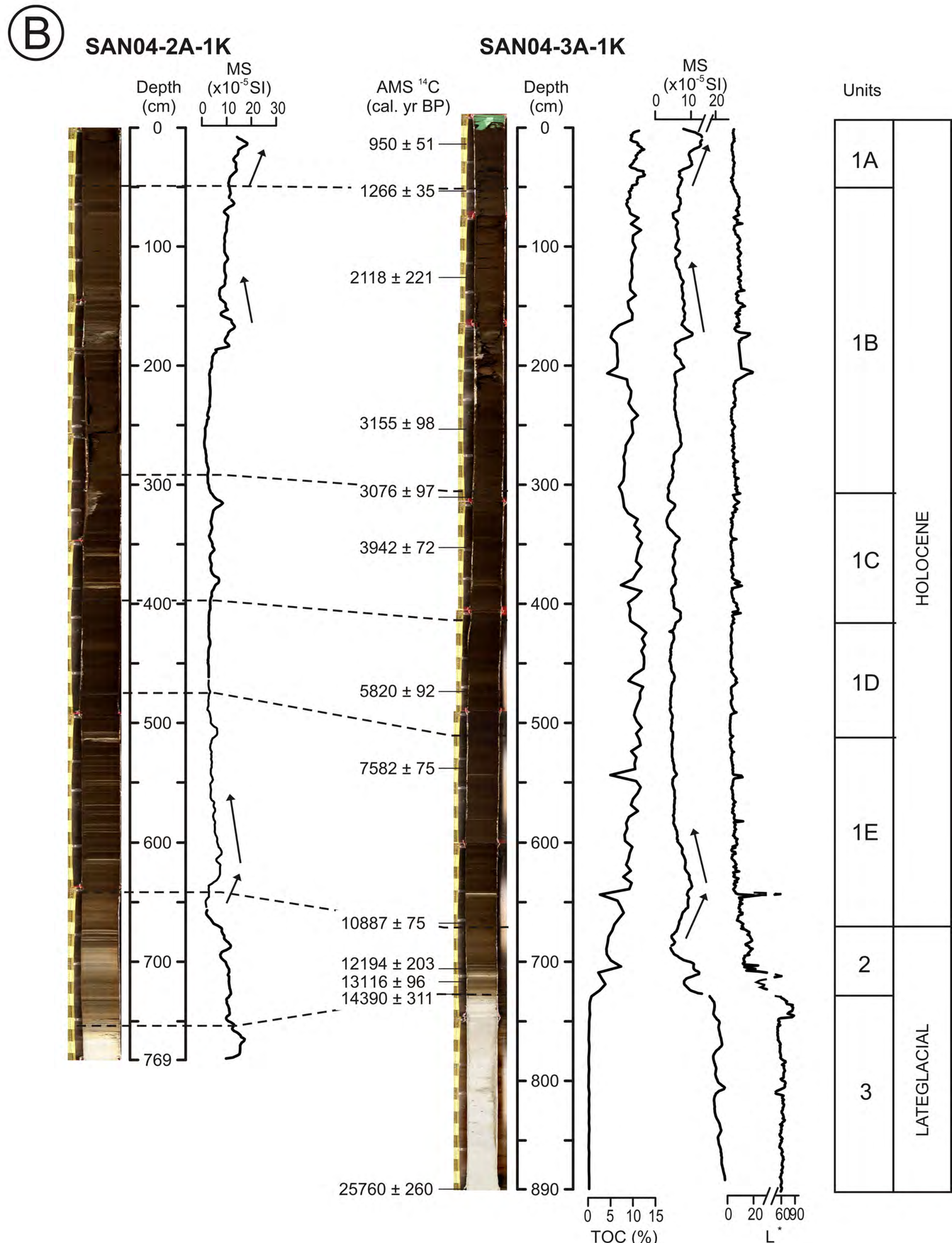
B
SAN04-2A-1K
Depth (cm)
MS (x10-5SI)
0 10 20 30
0
100
200
300
400
500
600
700
769
SAN04-3A-1K
AMS 14C (cal. yr BP)
Depth (cm)
MS (x10-5SI)
0 10 20
950 ± 51
1266 ± 35
2118 ± 221
3155 ± 98
3076 ± 97
3942 ± 72
5820 ± 92
7582 ± 75
10887 ± 75
12194 ± 203
13116 ± 96
14390 ± 311
25760 ± 260
0
100
200
300
400
500
600
700
800
890
0 5 10 15
TOC (%)
0 20 60 90
L*
Units
1A
1B
1C
1D
1E
2
3
HOLOCENE
LATEGLACIAL

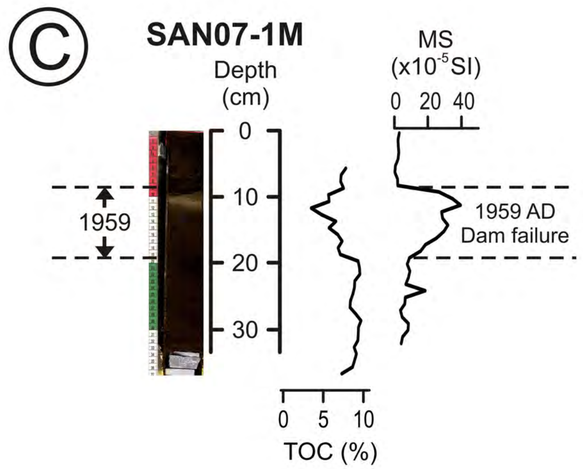
C
SAN07-1M
Depth (cm)
MS (x10-5SI)
0 20 40
1959
1959 AD
Dam failure
0
10
20
30
0 5 10
TOC (%)

Fig. 4

A

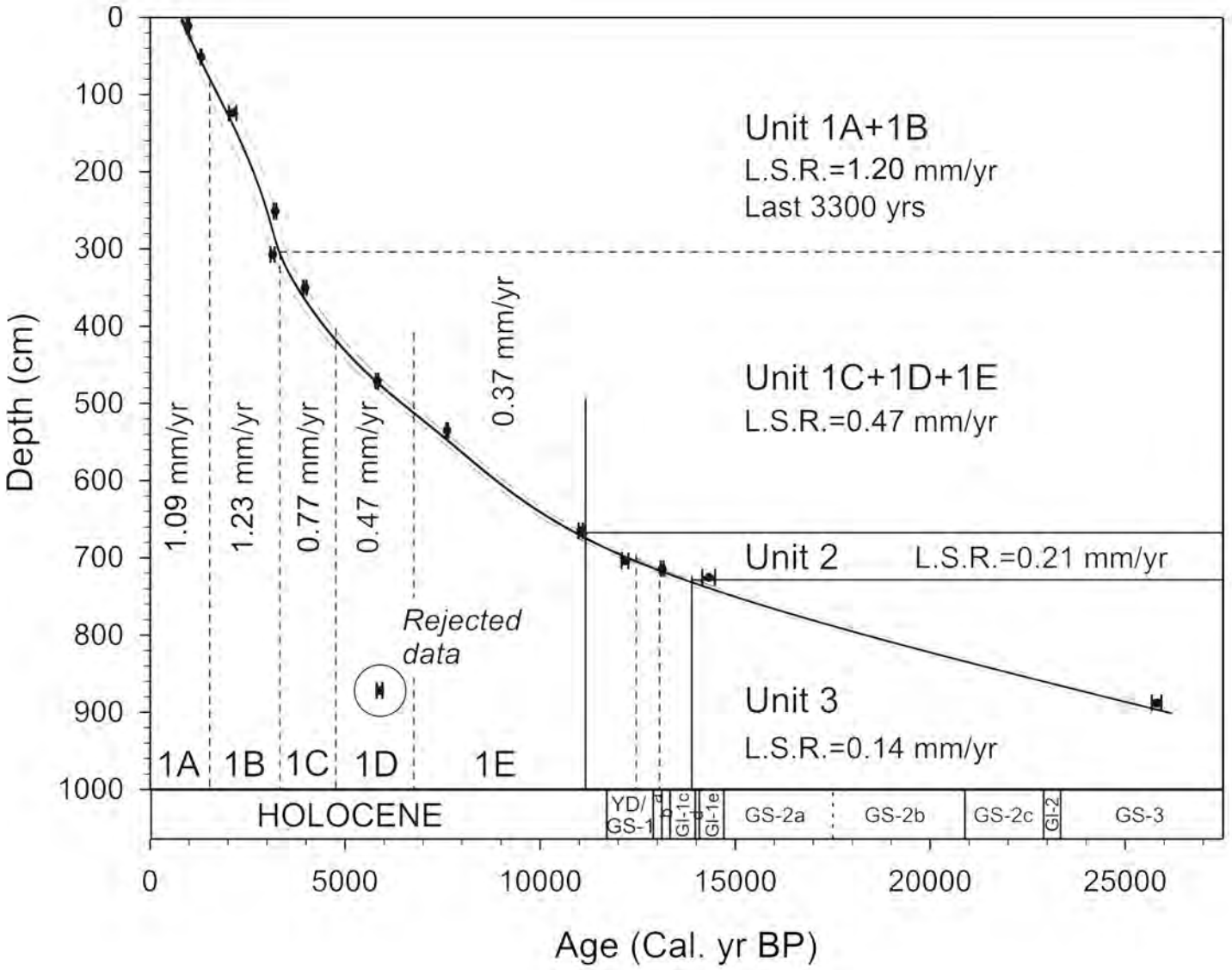
Depth (cm)
0
100
200
300
400
500
600
700
800
900
1000
Unit 1A+1B
L.S.R.=1.20 mm/yr
Last 3300 yrs
Unit 1C+1D+1E
L.S.R.=0.47 mm/yr
Unit 2
L.S.R.=0.21 mm/yr
Unit 3
L.S.R.=0.14 mm/yr
1.09 mm/yr
1.23 mm/yr
0.77 mm/yr
0.47 mm/yr
0.37 mm/yr
Rejected data
1A
1B
1C
1D
1E
HOLOCENE
YD/ GS-1
a
b
GI-1c
a
GI-1e
GS-2a
GS-2b
GS-2c
GI-2
GS-3
0
5000
10000
15000
20000
25000
Age (Cal. yr BP)

B

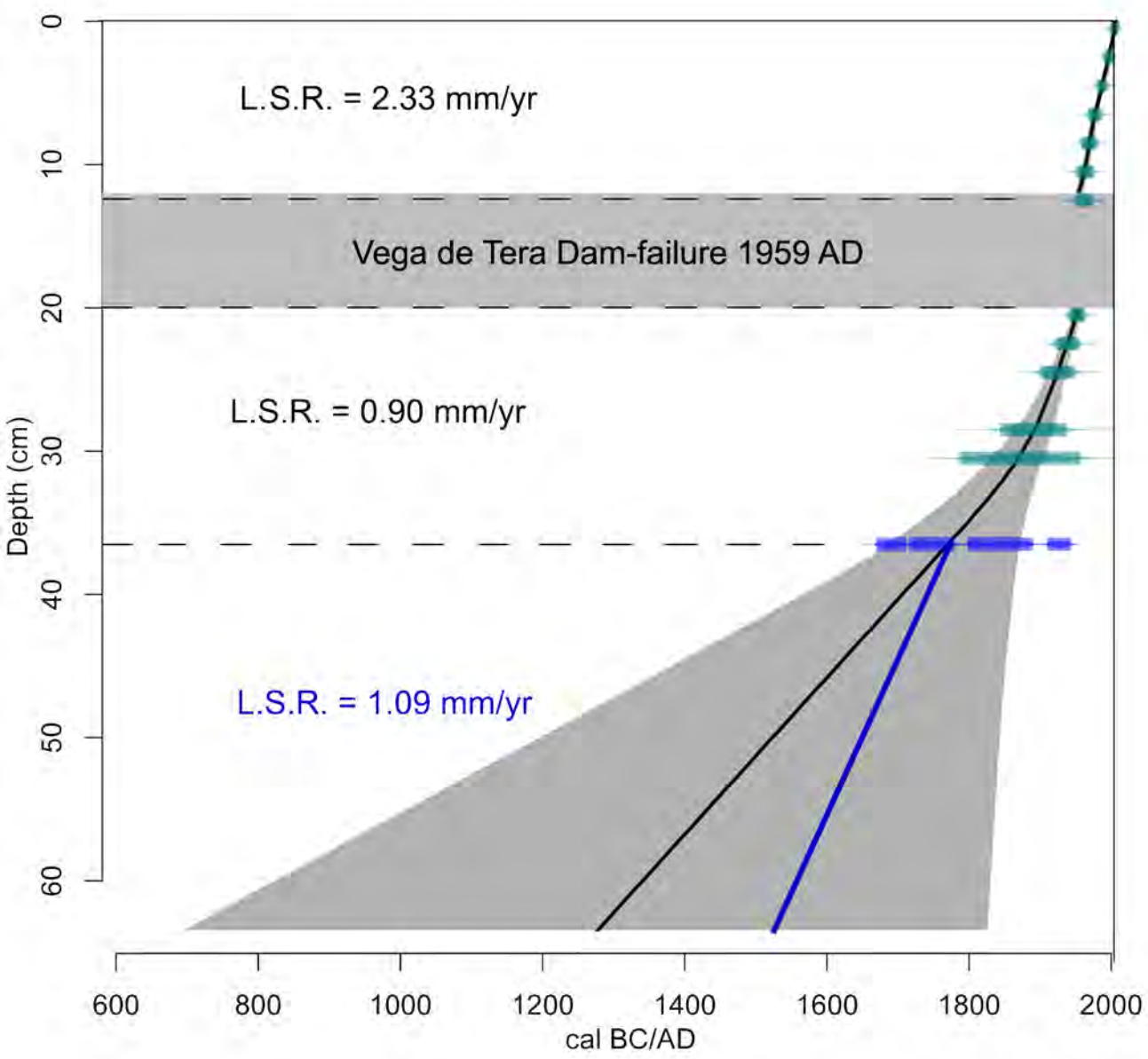
Depth (cm)
0
10
20
30
40
50
60
L.S.R. = 2.33 mm/yr
Vega de Tera Dam-failure 1959 AD
L.S.R. = 0.90 mm/yr
L.S.R. = 1.09 mm/yr
600
800
1000
1200
1400
1600
1800
2000
cal BC/AD

C

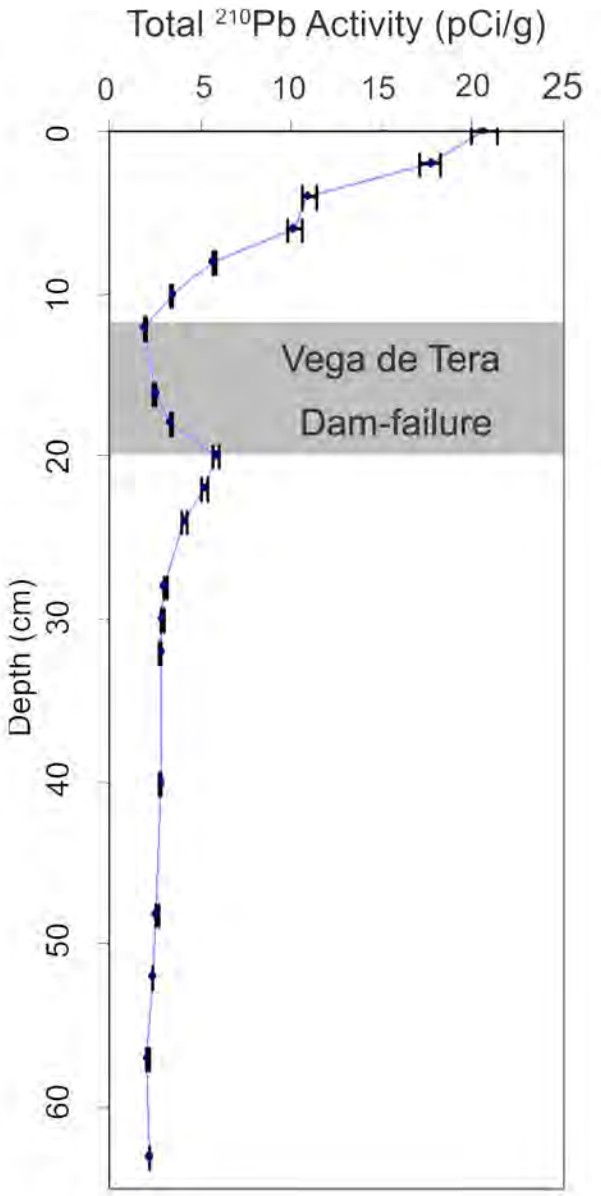
Total ^{210}Pb Activity (pCi/g)
0
5
10
15
20
25
Depth (cm)
0
10
20
30
40
50
60
Vega de Tera
Dam-failure

Fig. 5

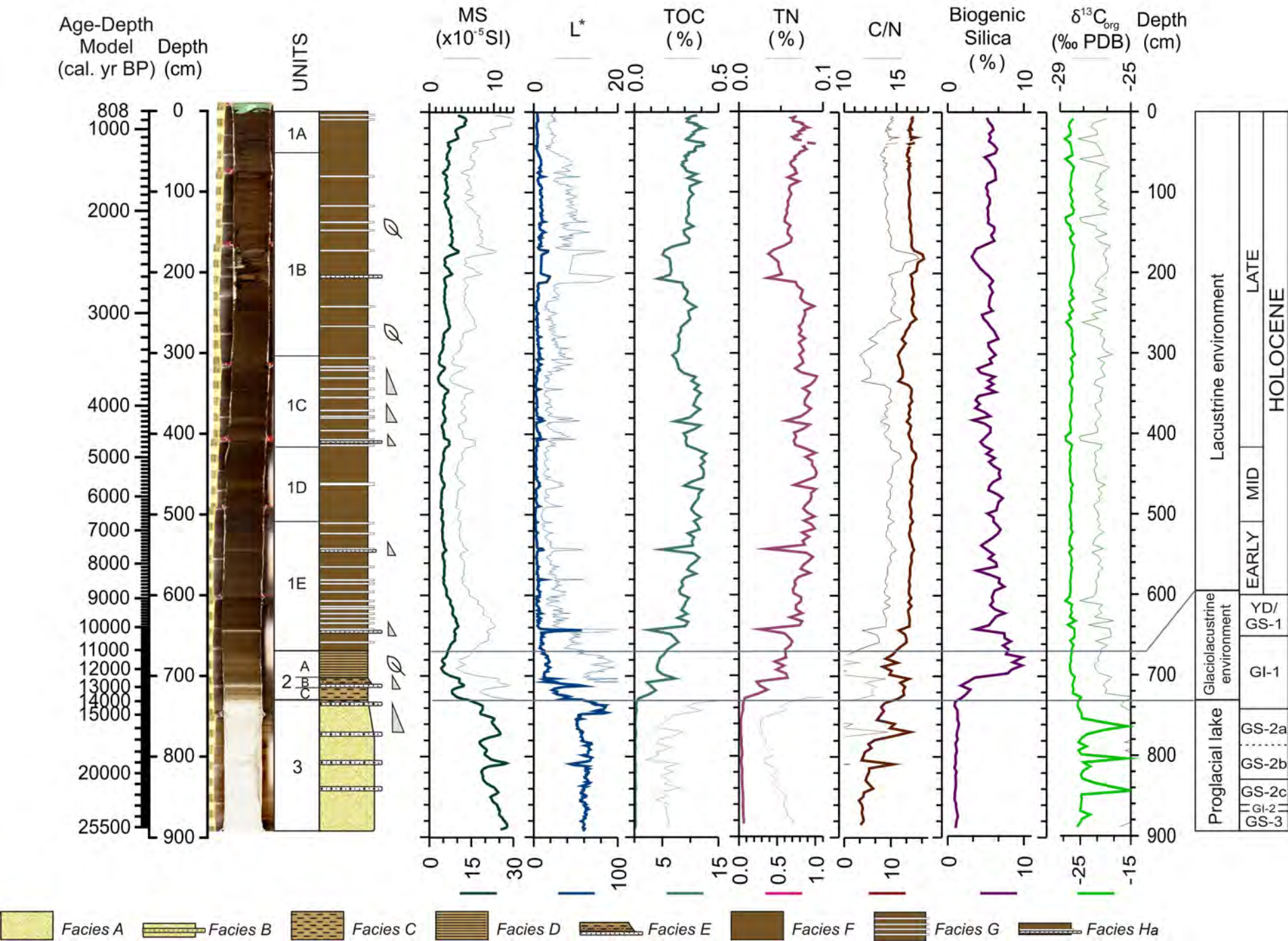
Age-Depth Model (cal. yr BP)
Depth (cm)
UNITS
1A
1B
1C
1D
1E
2
A
B
C
3
MS (x10⁻⁵SI)
L*
TOC (%)
TN (%)
C/N
Biogenic Silica (%)
δ13Corg (‰ PDB)
Depth (cm)
Lacustrine environment
Glaciolacustrine environment
Proglacial lake
HOLOCENE
LATE
MID
EARLY
YD/ GS-1
GI-1
GS-2a
GS-2b
GS-2c
GI-2
GS-3
Facies A
Facies B
Facies C
Facies D
Facies E
Facies F
Facies G
Facies Ha

Fig. 6

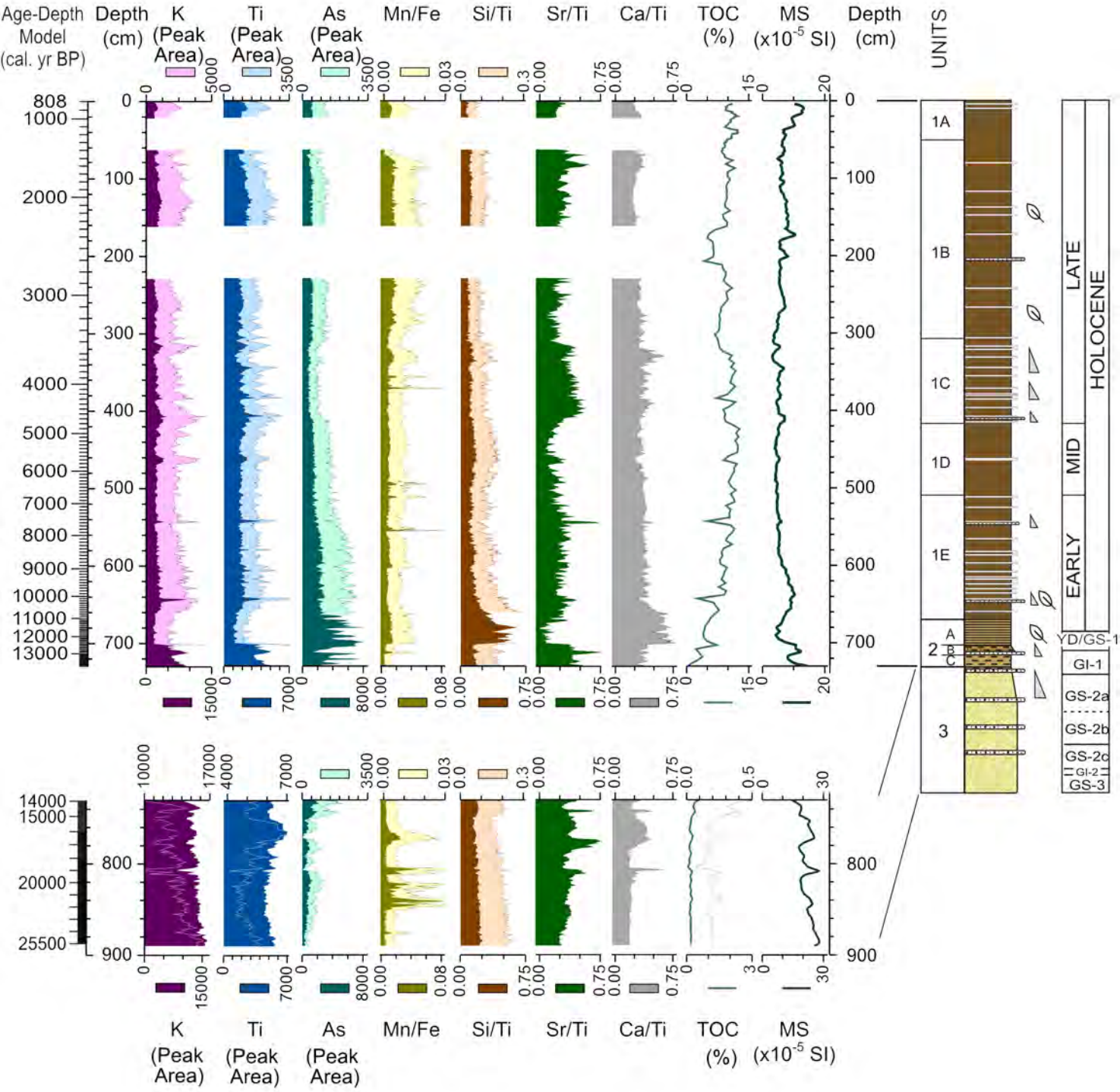
Age-Depth Model (cal. yr BP)
Depth (cm)
K (Peak Area)
Ti (Peak Area)
As (Peak Area)
Mn/Fe
Si/Ti
Sr/Ti
Ca/Ti
TOC (%)
MS (x10-5 SI)
Depth (cm)
UNITS
1A
1B
1C
1D
1E
2
A
B
C
3
LATE
MID
EARLY
HOLOCENE
YD/GS-1
GI-1
GS-2a
GS-2b
GS-2c
GI-2
GS-3

Fig. 7.

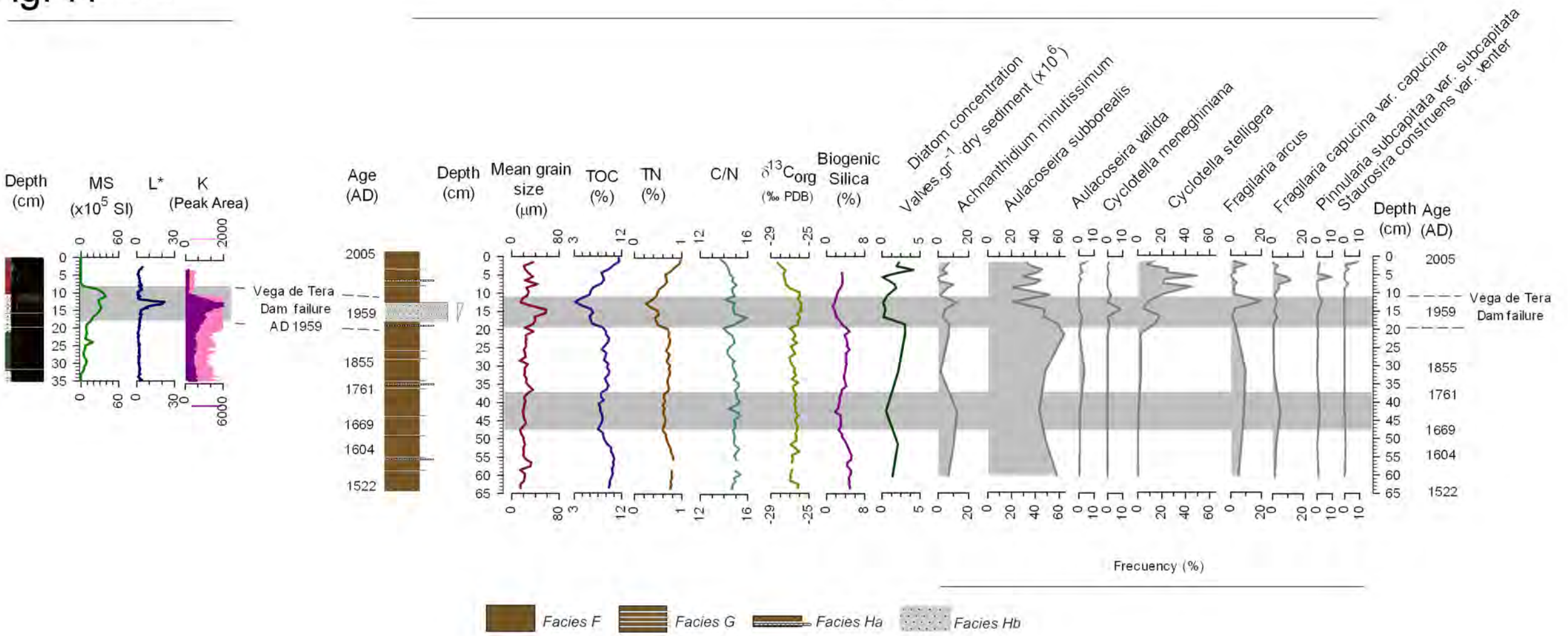
SAN07-1M
SAN07-2M
Depth (cm)
MS (x10^5 SI)
L*
K (Peak Area)
Age (AD)
Vega de Tera Dam failure AD 1959
Depth (cm)
Mean grain size (μm)
TOC (%)
TN (%)
C/N
$\delta^{13}C_{org}$ (‰ PDB)
Biogenic Silica (%)
Diatom concentration Valves.gr^{-1}.dry sediment (x10^6)
Achnanthidium minutissimum
Aulacoseira subborealis
Aulacoseira valida
Cyclotella meneghiniana
Cyclotella stelligera
Fragilaria arcus
Fragilaria capucina var. capucina
Pinnularia subcapitata var. subcapitata
Staurosira construens var. venter
Depth (cm)
Age (AD)
Vega de Tera Dam failure
Frecuency (%)
Facies F
Facies G
Facies Ha
Facies Hb

Fig. 8.

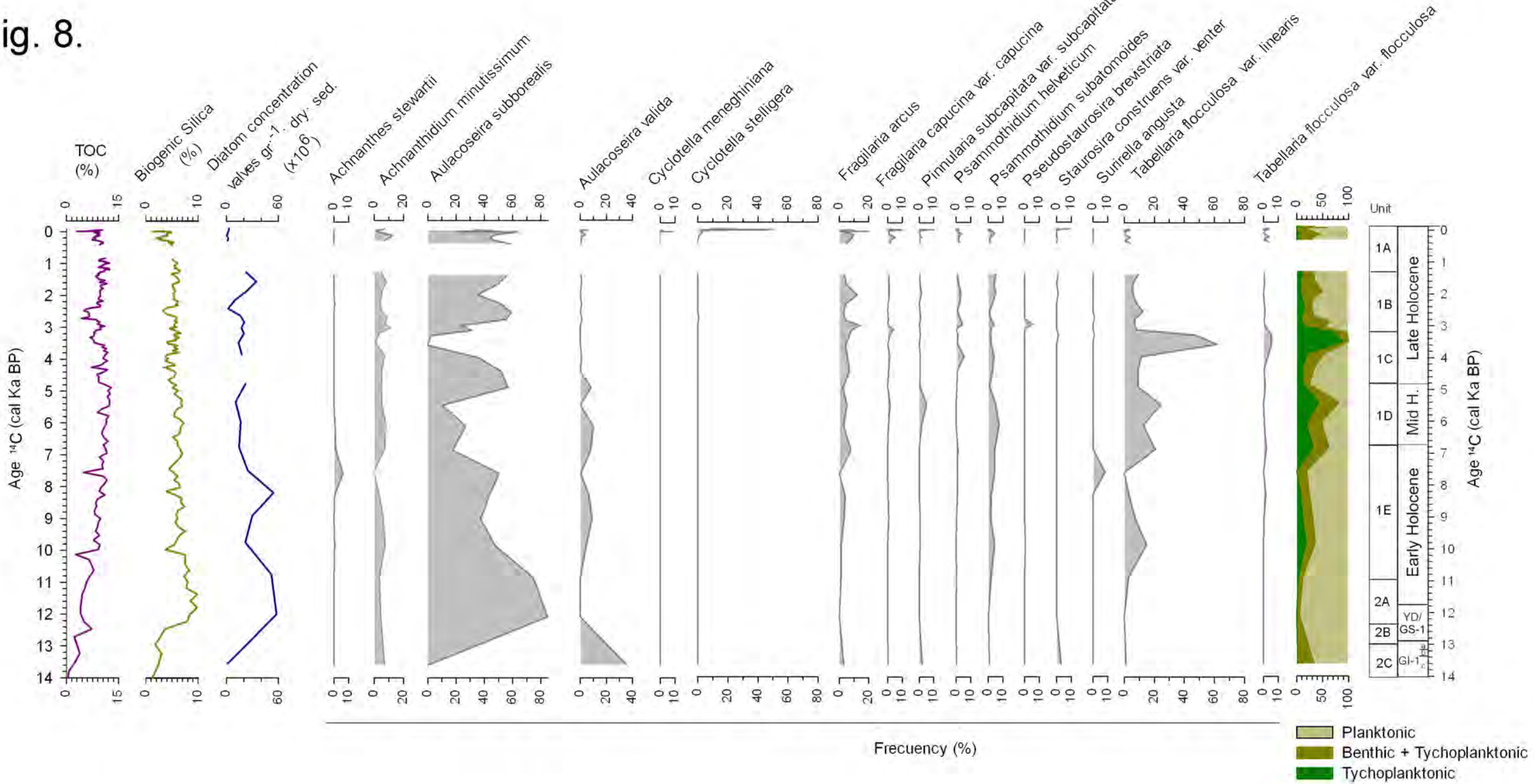
TOC (%)
Biogenic Silica (%)
Diatom concentration valves gr-1 dry sed. (x10^6)
Achnanthes stewartii
Achnanthidium minutissimum
Aulacoseira subborealis
Aulacoseira valida
Cyclotella meneghiniana
Cyclotella stelligera
Fragilaria arcus
Fragilaria capucina var. capucina
Pinnularia subcapitata var. subcapitata
Psammothidium helveticum
Psammothidium subatomoides
Pseudostaurosira brevistriata
Staurosira construens var. venter
Surirella angusta
Tabellaria flocculosa var. linearis
Tabellaria flocculosa var. flocculosa
Age 14C (cal Ka BP)
Unit
1A
1B
1C
1D
1E
2A
2B
2C
Late Holocene
Mid H.
Early Holocene
YD/ GS-1
GI-1
Frecuency (%)
Planktonic
Benthic + Tychoplanktonic
Tychoplanktonic

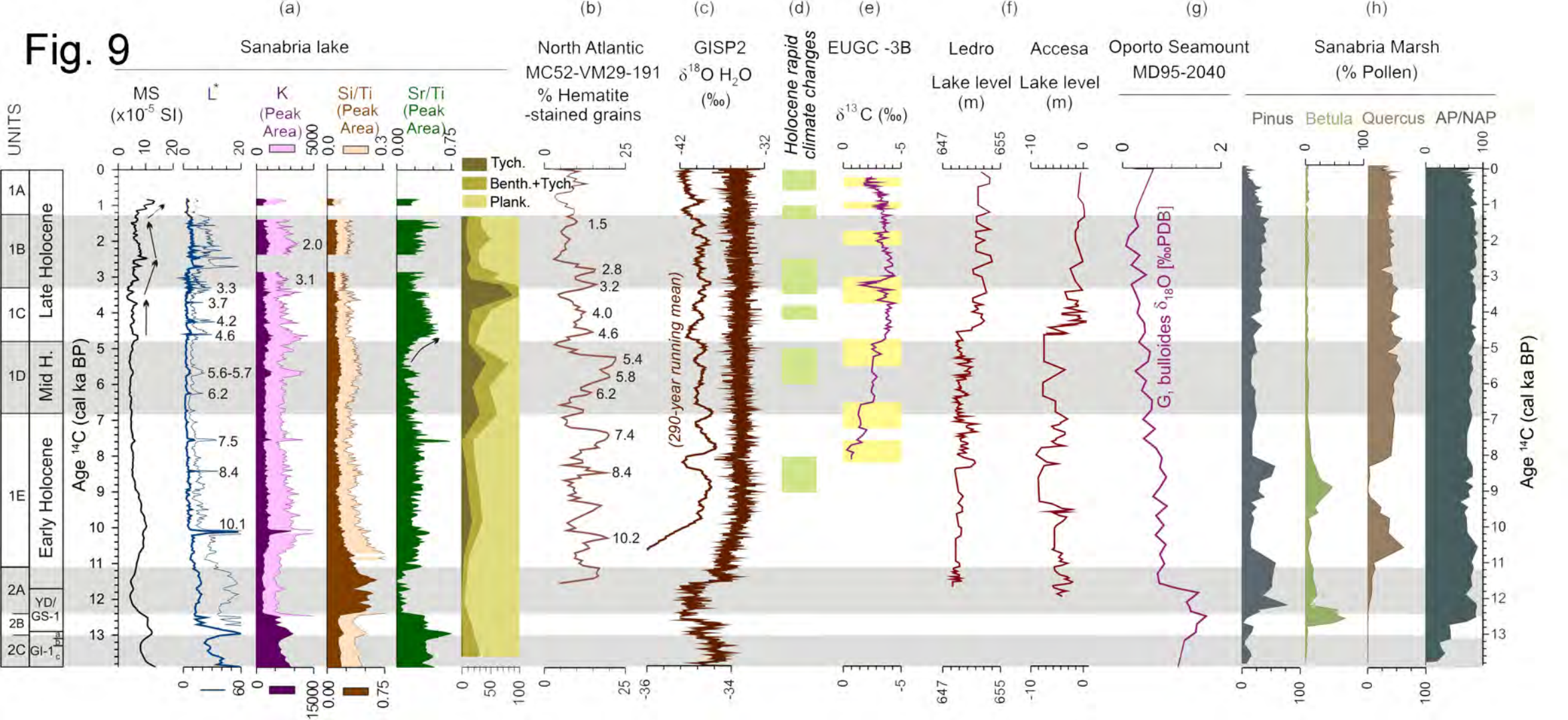
Fig. 9
(a)
(b)
(c)
(d)
(e)
(f)
(g)
(h)
Sanabria lake
MS (x10^{-5} SI)
L*
K (Peak Area)
Si/Ti (Peak Area)
Sr/Ti (Peak Area)
Tych.
Benth.+Tych.
Plank.
North Atlantic MC52-VM29-191 % Hematite -stained grains
GISP2 $\delta^{18}O$ H_2O (‰)
(290-year running mean)
Holocene rapid climate changes
EUGC -3B $\delta^{13}C$ (‰)
Ledro Lake level (m)
Accesa Lake level (m)
Oporto Seamount MD95-2040
G. bulloides $\delta_{18}O$ [‰PDB]
Sanabria Marsh (% Pollen)
Pinus
Betula
Quercus
AP/NAP
UNITS
1A
1B
1C
1D
1E
2A
2B
2C
Late Holocene
Mid H.
Early Holocene
YD/ GS-1
GI-1
Age ^{14}C (cal ka BP)
1.5
2.0
2.8
3.1
3.2
3.3
3.7
4.0
4.2
4.6
5.4
5.6-5.7
5.8
6.2
7.4
7.5
8.4
10.1
10.2